Palaeoenvironmental and palaeoecological reconstructions based on oxygen, carbon and sulfur isotopes of Early Permian shark spines from the French Massif central

Vincent Luccisano, Gilles Cuny, Alan Pradel, François Fourel, Christophe Lécuyer, Jean-Marc Pouillon, Kathleen Lachat, Romain Amiot

Palaeoenvironmental and palaeoecological reconstructions based on oxygen, carbon and sulfur isotopes of Early Permian shark spines from the French Massif central

Vincent Luccisano[1,2*], Gilles Cuny[2], Alan Pradel[3], François Fourel[2], Christophe Lécuyer[1], Jean-Marc Pouillon[4], Kathleen Lachat[1], Romain Amiot[1]

[1]Univ Lyon, UCBL, ENSL, UJM, CNRS, LGL-TPE, F-69622, Villeurbanne, France;

[2]Univ Lyon, Université Claude Bernard Lyon 1, CNRS, ENTPE, UMR 5023 LEHNA, F-69622, Villeurbanne, France;

[3]CR2P - Centre de Recherche en paléontologie - Paris ; Muséum National d'Histoire Naturelle - Centre National de la Recherche Scientifique- Sorbonne Université. France;

[4]Rhinopolis Association, 179 rue des Plattières 38300 Nivolas Vermelle/BP 39 03800 Gannat, France.

RH: Isotopic compositions of French Permian aquatic faunas

*Corresponding author. Email: vincent.luccisano@gmail.com

Abstract

The palaeoecology of the Xenacanthiformes (Chondrichthyes) is still a matter of discussion. Historically considered as freshwater organisms, hypotheses of euryhaline ecology including migratory behaviour were recently proposed based on the histology of their dorsal spines. However, recent studies still argued for a full freshwater ecology based on the geochemical compositions of their teeth. Their ecology is particularly interesting to investigate for those coming from the environmentally ambiguous Early Permian intra-mountainous localities of Buxières-les-Mines (Bourbon-l'Archambault Basin, Allier) and the Muse oil-shale bed (OSB) (Autun Basin, Saône-et-Loire) from the French Massif central. These two localities were interpreted as freshwater settings but doubts on marine influences exist. To assess their palaeoenvironment and the palaeoecology settings based on xenacanthiforms occurrences, we have analysed the stable isotope compositions ($\delta^{18}O$, $\delta^{13}C$ and $\delta^{34}S$) of the bioapatite of their vertebrate faunas. From these stable isotope compositions, we interpret that Buxières-les-Mines was a large and deep freshwater lake, equivalent to the modern Indonesian Lake Matano, whereas the Muse OSB is interpreted as a shallow tropical lake with drying up events, equivalent to the Lake Punta Laguna, Amazonia or the Lake Tanganyika, Africa. The oxygen isotope compositions of the xenacanth dorsal spines of Buxières-les-Mines are relatively constant from the apex to the base. Such uniform isotopic compositions recorded during the life of xenacanths support either their sedentary lifestyle or stenohalinity. The apparent ability of small xenacanthiforms to endure drying up, as shown by the variations in isotope composition of the Muse OSB specimens, could explain their resilience during the Early Permian whereas Carboniferous xenacanthiforms occurring in large lake and river systems almost disappeared.

Keywords: Stable isotope; geochemistry; Xenacanthiformes; late Palaeozoic; dorsal spine

1. Introduction

Xenacanthiformes is an order of Palaeozoic chondrichthyans characterised by an eel-like body, diplodont teeth and an ever-growing dorsal spine (e.g. Zangerl 1981; Ginter et al., 2010). It is divided into two families (e.g. Ginter et al., 2010): the Diplodoselachidae that exhibit a rounded dorsal spine with two posterior rows of denticles whereas the Xenacanthidae have a dorso-ventrally compressed dorsal spine which bears two lateral rows of denticles.

Most of the time, they have been recovered from ancient lacustrine or palustrine deposits (Zangerl, 1981; Compagno, 1990; Kriwet et al., 2008). Consequently, some authors (e.g. Schneider et al., 2000; Fischer et al., 2013, 2014; Štamberg et al., 2016) have interpreted them as a proxy of freshwater environments. However, numerous studies (Schultze, 1985, 1995, 1998, 2009, 2013; Olson, 1989; Soler-Gijón, 1993; Johnson, 1999; Soler-Gijón and Moratalla, 2001; Schultze and Soler-Gijón, 2004; Hampe et al., 2006; Laurin and Soler-Gijón, 2010; Carpenter et al., 2011; Beck et al., 2016) questioned their full freshwater-adaptation and argued in favour of a possible euryhaline ecology.

To test the different hypotheses concerning their environmental adaptations, recent studies have investigated the phosphate oxygen isotope composition ($\delta^{18}O_p$) of teeth from some Carboniferous and Permian xenacanthiforms from North America and Europe (Fischer et al., 2013, 2014). Xenacanthiforms were thus interpreted as full freshwater organisms living in environments experiencing significant drying events. However, other recent studies (e.g. Soler-Gijón and Moratalla, 2001; Schultze and Soler-Gijón, 2004; Hampe et al., 2006; Schultze, 2009; Laurin and Soler-Gijón, 2010; Carpenter et al., 2011) advocated for an euryhaline behaviour. These interpretations were supported by conclusions of Soler-Gijón (1999) and Beck et al., (2016) who focused on the histological structure of the dorsal spine of American and European *Orthacanthus* and who argued for an euryhaline ecology with

diadromous and catadromous migrations. These conflicting interpretations of xenacanthiforms palaeoecology emphasise the need to provide new investigations on this topic.

This is particularly true for xenacanthiforms from environmentally ambiguous basins like that of Bourbon-l'Archambault (Allier, France) in the French Massif central. Fischer et al. (2013) interpreted the $\delta^{18}O_p$ of teeth and dorsal spines of *Orthacanthus buxieri* from the Buxières-les-Mines locality in agreement with a freshwater living environment. However, Schultze and Soler-Gijón (2004) and Schultze (2009) listed faunal components of nearby localities from the French Massif central that could indicate a probable marine influence. In addition, the palaeoenvironment of the nearby Muse oil-shale bed (OSB) locality in the Autun Basin (Saône-et-Loire, France) has been widely investigated by Mercuzot (2020) and Mercuzot et al. (2022) from a sedimentological point of view. Doubts persist for this locality, which has also provided xenacanthiform remains. Depending on the used methods, the Muse OSB can be considered as a distal or coastal freshwater lake, but none of these hypotheses have been tested by geochemical analyses on xenacanthiform hard tissues up to now.

In this work, we test the hypothesis of a strict freshwater palaeoecology of the Xenacanthiformes from Buxières-les-Mines and the Muse OSB. We investigate the phosphate oxygen ($\delta^{18}O_p$), carbonate oxygen and carbon ($\delta^{18}O_c$ and $\delta^{13}C_c$) and the sulfur isotope compositions ($\delta^{34}S$) of the bioapatite along their dorsal spines in order to define 1) their living environment and 2) its potential changes during their lifetime. To better constrain the environmental reconstruction, we also investigated the whole associated aquatic vertebrate faunas composed of acanthodian fin spines, actinopterygian ganoid scales and temnospondyl bones.

2. Geological context

The Bourbon-l'Archambault Basin is located in the Northern Massif central (Fig. 1C; Allier, France; Châteauneuf 1980; Châteauneuf and Farjanel 1989) and is part of a large set of Carboniferous-Permian non-marine basins (Fig. 1A; Gand et al., 2015, 2017). It is structurally divided into two sub-basins (Châteauneuf and Farjanel, 1989; Steyer et al., 2000): the Aumance sub-basin in the West and the Souvigny sub-basin in the East. The sedimentary deposits, which are mostly composed of conglomerates, alluvial arkoses, palustrine coal seams, bituminous black shales, fluvial sandstones and thin pyroclastic horizons (Roscher and Schneider, 2006), extend stratigraphically from the Late Carboniferous to the Triassic (e.g. Steyer et al., 2000). For some authors (Roscher and Schneider, 2006; Steyer et al., 2000), this basin is characteristic of a freshwater environment, even if some doubts remain about potential marine influences (Schultze and Soler-Gijón, 2004; Schultze, 2009).

The former open-cast coal mine of Buxières-les-Mines is a fossiliferous locality located in the southern part of the Aumance sub-basin (Fig. 1C; Steyer et al., 2000). Stratigraphically (Fig. 1E), Buxières-les-Mines is situated in the Supra-Buxières Member in the upper part of the Buxières Formation (Steyer et al., 2000). Even if the Carboniferous-Permian transition is poorly known in this basin, the Buxières-les-Mines locality has always been considered as Early Permian deposits (Roscher and Schneider, 2006; Schneider and Werneburg, 2006; Steyer et al., 2000). Correlated with the lower 'Autunian' local age (Debriette, 1992; Steyer et al., 2000), the Buxières Formation extends from the latest Asselian to the Middle Sakmarian, (Roscher and Schneider 2006; Schneider and Werneburg 2006). Its geological age remains to be refined; however, the volcanic tuffs 'Lien Blanc' and 'Lien Vert' have been radiometrically dated at 294.6 ± 3.2 Ma (Ducassou et al., 2018) and at approximatively 298 Ma (M. Mercuzot, pers. comm., 2023), respectively, which implies an early to late Asselian age for this locality. The palaeoenvironment of Buxières-les-Mines could represent lacustrine or palustrine environments, which experienced several drying

events (Kaulfuß, 2003) without direct evidence of marine influences, contrary to Schultze and Soler-Gijón's (2004) and Schultze's (2009) opinions for all the basins of the Northern Massif central.

The Autun Basin is a half-graben basin, oriented West-East, located in the Northern Massif central (Fig. 1B; Saône-et-Loire, France; Gand et al., 2015, 2017). It is divided into four formations: Igornay and Muse formations constituting the lower 'Autunian' (upper Gzhelian to lower Asselian), and Surmoulin and Millery formations corresponding to the upper 'Autunian' (post-Assselian; Pruvost, 1942). The basin is interpreted as representing fluvio-lacustrine environments (Pruvost, 1942; Marteau, 1983; Mercuzot, 2020; Mercuzot et al., 2022).

The Muse OSB is located in the Muse Formation (Gand et al., 2011, 2015, 2017; Pellenard et al., 2017). It is mainly composed of oil-shale beds with intercalations of volcanic tonsteins (Fig. 1E). Two tonsteins were radiometrically dated at 298.05 ± 0.39 Ma and 298.57 ± 0.38 Ma (upper part of the Muse OSB stratigraphy in Pellenard et al. [2017]). The Muse OSB is therefore dated as lower Asselian (lowermost Permian) in age. Mercuzot (2020) assigned the sedimentary deposits to a palustrine environment that corresponds to a coastal freshwater lake.

3. Material and methods

3.1. $\delta^{18}O_p$ analysis

Bioapatite samples were treated following a previously described wet chemistry protocol (Crowson et al., 1991; Lécuyer et al., 1993). This protocol consists of the isolation of the phosphate ions (PO_4^{3-}) from bioapatite using acid dissolution and anion-exchange resin and precipitated as silver phosphate (Ag_3PO_4) crystals. For each sample, between 10 and 30 mg of dentine powder was dissolved in 2 ml of 2 M HF for 24hrs. The CaF_2 residue was separated by centrifugation and the solution was neutralized by adding 2.2 ml of 2 M KOH.

Amberlite™ IRN 78 anion-exchange resin (2.5 ml) was added to the solution to separate the PO_4^{3-} ions. After 24 h, the solution was rinsed with deionized water and the resin was eluted with 27.5 ml of 0.5 M NH_4NO_3. After 4 h, 0.5 ml of NH_4OH and 15 ml of an ammoniacal solution of $AgNO_3$ were added and the samples were placed in a thermostated bath at 68°C for 7 h, allowing the precipitation of Ag_3PO_4 crystals.

Oxygen isotope compositions were measured using a high-temperature pyrolysis technique involving a VarioPYROcube™ Elemental Analyser (Elementar GmbH) based on 'purge and trap' technology interfaced in Continuous Flow mode with an Isoprime™ Isotopic Ratio Mass Spectrometer (Elementar UK Ltd) using the protocol described in Fourel et al. (2011). For each sample, 5 aliquots of 300 μg of Ag_3PO_4 were mixed with 400 μg of carbon black powder and loaded in 3.5x5 mm silver foil capsules. Pyrolysis was performed at 1450°C. Measurements were calibrated against NBS120c (natural Miocene phosphorite from Florida) and NBS127 (barium sulfate, $BaSO_4$). The certified $\delta^{18}O$ value of NBS120c was fixed at 21.7‰ (Lécuyer et al., 1993; Halas et al., 2011) and the $\delta^{18}O$ of NBS127 set at the certified value of 9.3‰ (V-SMOW; Hut, 1987) for calibration of the unknown silver phosphate samples. Silver phosphate samples precipitated from standard NBS120c were repeatedly analysed ($\delta^{18}O_p$ = 21.7‰; 1σ = 0.2; n = 20) along with the silver phosphate samples derived from fossil bioapatites to ensure that no isotopic fractionation occurred during the wet chemistry. In this manuscript we have used the classical "permil" notation (‰). For $^{18}O/^{16}O$ delta notation, the reference was V-SMOW. $\delta^{18}O_p$ notation means delta notation versus V-SMOW for phosphate samples.

3.2. $\delta^{18}O_c$ and $\delta^{13}C_c$ analyses

To remove potential organic contaminants and secondarily precipitated calcite, bioapatite samples were pre-treated following the protocol of Koch et al. (1997). About 10 mg

of bioapatite powder was washed with a 2% NaOCl solution, followed by a 0.1 M acetic acid solution. Each treatment lasted for 24 h and samples were rinsed 5 times with distilled water between treatments. Pre-treated powders were collected after 24 h of air-drying at 40°C.

Carbon and oxygen isotope compositions were measured using an isoFLOW™ system connected on-line in continuous flow mode to a precisION™ mass spectrometer (Elementar UK). For each sample, three aliquots of 1 to 2 mg of pre-treated bioapatite powder were loaded in LABCO Exetainer® 3.7 ml soda glass vials, round bottomed with Exetainer caps, and were reacted with anhydrous phosphoric acid. The reaction took place at 90°C in a temperature regulated sample tray. The CO_2 gas generated during the acid digestion of the carbonate sample was then transferred to the mass spectrometer via the centrION™ interface. Calibrated CO_2 gas was used as the monitoring gas. For bioapatite, the acid fractionation factor α (CO_2–apatite carbonate) of 1.00773 determined for the NBS120c phosphate rock reference material was used (Passey et al., 2007).

The calibrated materials used were Carrara marble ($\delta^{18}O_c = -1.84‰$, $\delta^{13}C_c = 2.03‰$; Fourel et al., 2016), NBS18 ($\delta^{18}O_c = -23.2‰$, $\delta^{13}C_c = -5.01‰$; Friedman et al., 1982; Hut, 1987; Stichler, 1995; Coplen et al., 2006) and NBS120c ($\delta^{18}O_c = -1.13‰$, $\delta^{13}C_c = -6.27‰$; Passey et al., 2007). Isotopic compositions are quoted in the standard δ notation relative to V-SMOW for oxygen and V-PDB for carbon.

3.3. $\delta^{34}S$ analysis

Sulfur isotope compositions of bioapatite samples were measured using a VarioPYROcube™ Elemental Analyser in NCS combustion mode based on ‘purge and trap’ technology, interfaced in continuous-flow mode with an Isoprime™ 100 Isotope Ratio Mass Spectrometer. The technique is fully described in Fourel et al. (2014). Bioapatite samples were analysed by weighing 3 aliquots of 5 mg of untreated apatite in tin foil capsules mixed

with 15 mg of pure tungsten oxide (WO_3) powder. Tungsten oxide is a powerful oxidant that ensures the full thermal decomposition of bioapatite sulfate into sulfur dioxide (SO_2) gas (Goedert et al., 2016).

Measurements were calibrated against IAEA-S-2 (silver sulfide, Ag_2S; $\delta^{34}S$ = 22.7‰; Stichler, 1995), IAEA-SO-5 (barium sulfate BaSO4; $\delta^{34}S$ = 0.5‰; Halas and Szaran 2001), and IAEA-SO-6 (barium sulfate BaSO4; $\delta^{34}S$ = −34.1‰; Halas and Szaran 2001), international standards (Halas and Szaran, 2001). For each analytical run of bioapatite samples, we have also analysed BCR32 samples as a compositional and isotopic standard (S% = 0.72, certified value; $\delta^{34}S$ = 18.4‰; Fourel et al., 2015; Goedert et al., 2016) to ensure that analytical conditions were optimal to perform sulfur isotope analyses on samples with low-sulfur content. The standard deviation of $\delta^{34}S$ measurements was better than 0.2‰. The VarioPYROcube™ Elemental Analyser is equipped with a Thermal Conductivity Detector (TCD) and was used to measure the sulfur content of the samples. For $^{34}S/^{32}S$ delta notation, the reference was V-CDT.

3.4. Palaeotemperatures

In primarily non-air-breathing vertebrates, the body temperature (T_b) is assumed to be similar to that of the surrounding water (T_w) (e.g. Haesemeyer, 2020). However, some large and active pelagic fishes, such as lamnid sharks, billfishes, tunas and oar fishes, are able to maintain higher T_b than their T_w (e.g. Carey and Teal, 1969; Goldman, 1997) as an adaptation to their high energy demands to perform long migration or move in the column water. However, the small sized aquatic vertebrates investigated in this study do not exhibit anatomical characters that correspond to this specific ecology. Moreover, xenacanths have been interpreted as potential fast-start swimmer like garpikes (Luccisano et al., 2021). Consequently, we consider that Xenacanthiformes, Acanthodii and Actinopterygii from

Buxières-les-Mines and the Muse OSB are assumed to have their T_b similar to that of their T_w. Furthermore, the $\delta^{18}O$ value of their body water ($\delta^{18}O_{bw}$) is considered to be equal to the $\delta^{18}O$ of ambient environment ($\delta^{18}O_w$) (Kolodny et al., 1983). In order to investigate the T_b, we use the fractionation equation adapted from the phosphate-water temperature scale established by Lécuyer et al. (2013) that relates the bioapatite phosphate $\delta^{18}O_p$ value to that of body water and body temperature and that is valid for a large range of aquatic vertebrates:

$$T_b(°C) = 117.4(\pm 9.8) - 4.5(\pm 0.43) \times \left(\delta^{18}O_p - \delta^{18}O_{bw}\right)$$

3.5. Sampling

All the material comes from Buxières-les-Mines and the Muse OSB. We have chosen to investigate the dorsal spines of Xenacanthiformes because they are heavily mineralized structures composed of dentine (Reif, 1978), which is known for being able to well-preserve isotope signals (e.g. Fischer et al., 2013). Furthermore, they are non-replaced structures with a continuous growth (Soler-Gijón, 1999; Beck et al., 2016) that allow variations in the isotope composition to be tracked during the lifespan of these organisms.

The xenacanthiform dorsal spine growth pattern (Fig. 2) has been discussed by Soler-Gijón (1999) and Beck et al. (2016). They showed that the growth took place by the addition of new proximal dentine layers. Thus, the oldest part of the dorsal spine is the apex, i.e. the interior of the distal part. As the pattern of the different growth layers of the xenacanthiform dorsal spines was not well-preserved, we sampled cf. *Triodus* sp. dorsal spines by cutting small sections all along the length of each spine in order to collect large enough amounts of bioapatite for the geochemical analyses (Fig. 2). For the cf. *Orthacanthus* sp. dorsal spine, we followed a similar protocol focusing on the most external part of the spine to minimise mixing of several growth layers (Fig. 2).

Following Jerve et al. (2017), the growth model of the acanthodian fin spines is more related to chondrichthyans than to osteichthyans, even though dentine growth layers were not identified in some extant (e.g. Maisey, 1979; Burrow et al., 2015, 2016) or extinct chondrichthyans (e.g. Maisey, 1978, 1982; Soler-Gijón, 1999; Beck et al., 2016). The acanthodian fin spine grows by implementation of new dentine material from the apex to the base. Consequently, the distal part of the fin spine is older than the base.

4. Results

4.1. Stable isotope values

The mean oxygen, carbon and sulfur isotope compositions of bioapatite phosphates and carbonates of each specimen are reported in Table 1 (see Table S1 for the detailed values of each sample). In the Muse OSB, the $\delta^{18}O_p$ values range from 17.3‰ to 25.1‰, the $\delta^{13}C_c$ from 3.3‰ to 5.9‰ and the $\delta^{34}S$ from 1.2‰ to 6.9‰. In Buxières-les-Mines, the $\delta^{18}O_p$ values range from 14.0‰ to 18.7‰, the $\delta^{13}C_c$ from –2.7‰ to 5.7‰ and the $\delta^{34}S$ from –20.3‰ to 7.9‰. Between the taxonomic groups, the temnospondyls from Buxières-les-Mines have the lowest $\delta^{18}O_p$ (15.1±0.6‰) and $\delta^{13}C_c$ (–2.6±0.1‰) values.

4.2. Isotopic variations along the spines

$\delta^{18}O_p$ values of cf. *Triodus* sp. (Fig. 3A) dorsal spines from the Muse OSB range from 17.3‰ to 25.1‰. Different trends of the $\delta^{18}O_p$ values are observed along the dorsal spine length. One dorsal spine (965a) shows no significant variations of the $\delta^{18}O_p$ values. For the three other ones, there is an increase in $\delta^{18}O_p$ values from the apex to the base. Specimen 943 shows an increase of almost 2‰ and of more than 4‰ in specimens 326 and 907b. For the two cf. *Orthacanthus* sp. dorsal spines from Buxières-les-Mines (Fig. 3B), $\delta^{18}O_p$ values range from 17.2‰ to 18.0‰ (D13) and from 16.2‰ to 17.1‰ (BX04). The $\delta^{18}O_p$ values tend to decrease from the apex to the base, they never exceed more than 18‰ and there is less than

277 1‰ difference between the highest and the lowest values. $\delta^{18}O_p$ values of cf. *Triodus* sp. from
278 Buxières-les-Mines (Fig. 3C) range from 15.9‰ to 18.6‰. Despite increasing (BX28) or
279 decreasing (D08), the $\delta^{18}O_p$ values within each dorsal spine do not vary more than 1‰ from
280 the apex to the base, excepted for two spines (D07 and D11). The latter and one cf.
281 *Orthacanthus* sp. (BX04) show a distinct decrease in $\delta^{18}O_p$ values in the distal half that can
282 reach more than 1‰ in D11.

283 In Buxières-les-Mines, $\delta^{13}C_c$ values of BX04 range from 0.9‰ to 1.9‰ with the
284 exception of the most proximal point (base of the dorsal spine) at almost 0‰ (Fig. 4B). The
285 variation seems to be cyclical. $\delta^{13}C_c$ values of D08 continuously decrease from the apex to the
286 base from 5.2‰ to 2.7‰. The $\delta^{34}S$ values of BX04 (Fig. 5) range from –6‰ to 3.8‰
287 following irregular cycles of decreases and increases with the highest values at the base of the
288 dorsal spine. For the other xenacanth and acanthodian spines (Fig. 5), the $\delta^{34}S$ values decrease
289 from the apex to the base.

290 Along the length of a same fin spine, the acanthodians from the Muse OSB and
291 Buxières-les-Mines do not show significant variations in their $\delta^{18}O_p$ (Fig. 6), $\delta^{13}C_c$ (Fig. 4A)
292 and $\delta^{34}S$ values (Fig. 5), i.e. less than 1‰. The only exception is the specimen (1924) from
293 the Muse OSB, in which the $\delta^{18}O_p$, $\delta^{13}C_c$ and $\delta^{34}S$ values decrease from the apex to the base.
294
295
296 **5. Discussion**
297 *5.1. Preservation of the original isotopic compositions of fossil bioapatite*

298 No method is available to formally demonstrate that the original isotopic composition
299 of the $\delta^{18}O_p$ is preserved in fossil bioapatite. However, several tests have been proposed. In
300 modern vertebrate skeletal tissues, and supposedly in fossil ones, phosphates and carbonates
301 of the bioapatite both precipitate near isotopic equilibrium with body water. Consequently,
302 $\delta^{18}O_p$ and $\delta^{18}O_c$ are positively correlated. Re-equilibration of both phosphate and carbonate

303 with diagenetic fluids is not expected because both have different isotopic exchange rates.
304 Moreover, it is expected that the $\delta^{18}O$ values of phosphate and associated apatite-bound
305 carbonate of fossil fishes and sharks follow the same trend observed in modern sharks and
306 mammals (e.g. Kolodny and Luz, 1991; Bryant et al., 1996; Iacumin et al., 1996; Vennemann
307 et al., 2001; Lécuyer et al., 2003). $\delta^{18}O_p$ and $\delta^{18}O_c$ values of vertebrates from Buxières-les-
308 Mines and the Muse OSB follow the distribution of modern and fossil sharks (Fig. 7). In
309 addition, the intra-site variability is congruent with the known measured biological variability
310 of the $\delta^{18}O_p$ values in modern shark teeth (Vennemann et al., 2001). Re-crystallisation and
311 diagenetic effect on dentine tissues should result in a homogenisation of the values, not
312 observed in Buxières-les-Mines and the Muse OSB.
313 Another evidence in favour of an original preservation of the $\delta^{18}O_p$ values is the
314 difference of almost 1.5‰ between exclusive aquatic (fishes) and semi-aquatic (amphibians)
315 vertebrates in Buxières-les-Mines (Table 1). As they have different physiologies and
316 ecologies, this difference is expected because of the different origin of their body water. For
317 these reasons, we can consider that the original oxygen isotopic signal could be preserved. We
318 compared the oxygen isotope composition of the $\delta^{18}O_p$ and the $\delta^{18}O_c$ values with the
319 carbonate content (CO_3^{2-} wt%) of each sample (Fig. 8). In modern sharks, the $\delta^{18}O_p$ values
320 can increase to 14.7‰ compared to the $\delta^{18}O_c$ values (Vennemann et al., 2001). Microbially-
321 induced diagenetic alteration has previously been shown to increase the offset between $\delta^{18}O_p$
322 and $\delta^{18}O_c$ values (e.g. Zazzo et al., 2004). The CO_3^{2-} wt% values of teeth and bones of
323 modern vertebrates range from 2 to 13.4 wt% (Brudefold and Soremark, 1967; Rink and
324 Schwarcz, 1995; Vennemann et al., 2001). The samples from Buxières-les-Mines and Muse
325 OSB have $\delta^{18}O_c$–$\delta^{18}O_p$ and CO_3^{2-} wt% values (see Table S1 for the detailed values) out of the
326 supposed diagenetic area, except for two samples. The latter, at 5.9 wt% and 7.7 wt%
327 respectively, are clearly outside the 0.4 wt% to 3.3 wt% range of the other values. Thus, we

assume that the oxygen and carbon isotope compositions of apatite carbonate preserved the original isotopic signal of the sampled data set.

The principal argument for the preservation of the isotopic composition of the $\delta^{13}C_c$ is the systematic and significant difference of at least 3‰ in $\delta^{13}C_c$ values between fish and amphibians in Buxières-les-Mines (Table 1). In the semi-terrestrial amphibians, the $\delta^{13}C_c$ values mainly may reflect those of the diet. In this case, the isotope fractionation depends on the digestive physiology (Passey et al., 2005). *A contrario*, for the fishes, the relationship between the $\delta^{13}C_c$ values and diet is influenced by significant amounts of carbon deriving from dissolved inorganic carbon of the ambient water (McConnaughey et al., 1997, Thorrold et al., 1997), resulting in higher $\delta^{13}C_c$ values (Santos et al., 2011).

As far as the $\delta^{34}S$ values are concerned, secondary minerals can precipitate at the surface or within the bones during fossilisation and they would tend to increase the sulfur content of bones, which is lower than 0.6 weight% S (wt% S) in modern bioapatite (e.g. Goedert et al. 2018). The Muse OSB samples show globally lower wt% S (mean of 0.4 wt% S) than those of Buxières-les-Mines (mean of 1.1 wt% S). In the Muse OSB, acanthodians and actinopterygians have similar $\delta^{34}S$ values and sulfur contents that vary in a narrow range within each taxonomic groups (Fig. 9). In Buxières-les-Mines, the sample size is higher than in the Muse OSB. Consequently, for each common taxonomic groups, the variability in the $\delta^{34}S$ and wt% S values is higher in Buxières-les-Mines than in the Muse OSB (Fig. 9). However, the main part of the data ranging from -10‰ to 10‰ for $\delta^{34}S$ and from 0.1 wt% S to 2 wt% S for the sulfur content. Within temnospondyls and xenacanths, a few points show low $\delta^{34}S$ values for slightly higher wt% S. Consequently, these few samples are interpreted as diagenetically altered, whereas the remaining $\delta^{34}S$ measurements of Buxières-les-Mines are interpreted as reflecting the living environment of the studied vertebrates.

353 *5.2. Palaeoenvironmental reconstruction of Buxières-les-Mines and the Muse OSB*

354 *5.2.1. $\delta^{34}S$*

355 Seawater $\delta^{34}S$ value was close to 12‰ at the Carboniferous-Permian transition
356 (Claypool et al., 1980), highly contrasting with the modern $\delta^{34}S$ value of 20.99±0.25‰ (Rees
357 et al., 1978; Paytan et al., 2020). Based on recent investigations conducted on modern and
358 fossil vertebrates from a broad phylogenetic context (Goedert, 2017; Goedert et al., 2018,
359 2020), the $\delta^{34}S$ value of vertebrate bioapatite is supposed to be close to that of their living
360 environment in the absence of sizable isotopic fractionation (0.5±2.4‰) between the animal
361 and its diet (Nehlich, 2015).

362 All the taxonomic groups from Buxières-les-Mines exhibit $\delta^{34}S$ values lower than
363 12‰ with variations from –6.0‰ to 9.6‰ for unaltered samples. The $\delta^{34}S$ values from the
364 Muse OSB range from 1.2‰ to 6.9‰. Those samples are depleted in heavy isotope by at least
365 3‰ and on average by 10‰ compared to seawater. This means that their sulfur content is
366 mainly derived from river input. To a lesser extent, brackish water could have influenced the
367 three highest $\delta^{34}S$ values from Buxières-les-Mines: 9.6‰ for an actinopterygian and 7.1‰
368 and 7.9‰ for two temnospondyls. In light of the bioapatite $\delta^{34}S$ values, the environment of
369 Buxières-les-Mines and the Muse OSB do not seem to have been subjected to significant
370 marine influences contrary to what was assumed in previous studies (e.g. Schultze and Soler-
371 Gijón 2004; Schultze, 2009).

372

373 *5.2.2. $\delta^{18}O_p$*

374 Conodont $\delta^{18}O_p$ values are considered to be relevant proxies of seawater temperatures
375 during the Palaeozoic (Joachimski et al., 2004, 2006, 2009; Trotter et al., 2008; Wenzel et al.,
376 2008; Chen et al., 2013). Consequently, we can consider that $\delta^{18}O_p$ values of the Early
377 Permian marine setting is close to 22‰ according to Chen et al. (2013). We therefore do not

agree with Fischer's et al. (2013) opinion who considered 18‰ as the lower limit for the $\delta^{18}O_p$ values of the Early Permian marine setting.

In Buxières-les-Mines, except for the temnospondyls, which have $\delta^{18}O_p$ values between 14.0‰ and 15.7‰, the aquatic vertebrate fauna, i.e. actinopterygians, acanthodians and xenacanthiforms, have $\delta^{18}O_p$ values ranging from 15.7‰ to 18.7‰ (Table S1). These values indicate a freshwater environment. Furthermore, highest $\delta^{18}O_p$ values, close to 19‰, are not positively correlated with $\delta^{34}S$ values (see Table S1), so that any potential marine influence is unlikely.

Strict aquatic vertebrates are supposed to be part of the same food web (Kriwet et al., 2008), but this does not mean that they share the same $\delta^{18}O_p$ values. There could be vertical water temperature gradients in lakes even if it is less marked in temperate lakes than in tropical ones (Lewis Jr, 1987). Temnospondyls have $\delta^{18}O_p$ values almost 2‰ lower than those measured in the other taxa of the faunal association (Table 1). This observation is congruent with an ecological partitioning due to their semi-terrestrial behaviour. Palynomorph assemblages indicate coal-swamp to mesoxerophytic environments, indicating the prevalence of humid conditions, at least at a seasonal scale (Paquette et al., 1980; Steyer et al., 2000). Therefore, temnospondyls could partly live in a humid tropical environment characterised by precipitation slightly or not ^{18}O-depleted relative to the global ocean. Another explanation could be provided by a high-altitude habitat where the depletion in heavy isotopes of waters increase with the related decrease in air temperature (Dansgaard, 1964). As modern giant salamanders can live up to 1,500 meters above sea level (Gang et al., 2004), it cannot be excluded that temnospondyls may have occupied similar habitats. To the contrary, the $\delta^{18}O_p$ values of aquatic taxa could derive from the lake water, which is under evaporation influences, and thus, had higher water $\delta^{18}O$ values. Consequently, the $\delta^{18}O_p$ values derived from precipitations exhibit lower values than those derived from lake water.

In the Muse OSB, the $\delta^{18}O_p$ values range from 17.3‰ to 25.1‰ for xenacanthiforms, from 19.3‰ to 21.3‰ for acanthodians and from 17.6‰ to 18.6‰ for actinopterygians. As for Buxières-les-Mines, most of them, lower or close to 22‰, can be interpreted as freshwater markers. However, the mean $\delta^{18}O_p$ value in the Muse OSB is higher (20.0‰) than that of Buxières-les-Mines (17.0‰) and numerous $\delta^{18}O_p$ values, especially in xenacanthiforms and acanthodians, are higher than 22‰ and up to 25.1‰. Permian conodont $\delta^{18}O_p$ is in the range of 21‰–23‰ and match some $\delta^{18}O_p$ values recorded in the Muse OSB. However, high $\delta^{18}O_p$ may reflect ^{18}O-enriched water due to large evaporation rates that commonly take place in arid environments. Such mechanisms can be favoured by monsoonal climates, which were supposed to occur in these low latitude tropical basins as postulated by Roscher and Schneider (2006) based on Parrish's (1993) and Kutzbach and Ziegler's (1994) modelling. Shallow tropical waters, such as swamps, lagoons or lakes, are characterised by a dry and a humid season, both being warm with a contrasted hydrological budget leading to $\delta^{18}O_p$ differences in the aquatic vertebrate fauna of up to 5‰ (Otero et al., 2010), which are in the range of the highest $\delta^{18}O_p$ values compared to the lowest ones. The highest $\delta^{18}O_p$ values are higher than those of the contemporaneous marine vertebrates and no sedimentological, palaeogeographical or geochemical (present $\delta^{34}S$ analyses) evidence agrees with a potential connection between the French Massif central basins and a marine environment. We therefore interpret the Muse OSB as a shallow freshwater environment recording extensive drying events.

5.2.3. $\delta^{13}C_c$

The $\delta^{13}C_c$ values of aquatic vertebrates of Buxières-les-Mines and the Muse OSB range from –0.8‰ to 7.0‰. These values are globally different from those recorded by the modern marine shark teeth. In the latter, $\delta^{13}C_c$ values range from –6.8‰ to 4.8‰

(Vennemann et al., 2001). Previous studies devoted to fossil and modern fishes (see Kolodny and Luz, 1991; Fricke et al., 1998; Vennemann et al., 2001; Amiot et al., 2010; Błażejowski et al., 2013; Goedert et al., 2016) showed that the $\delta^{13}C_c$ values of the apatite of freshwater and marine vertebrates can overlap and are not a good proxy for discriminating these two environments. However, Horton et al. (2015) showed, based on water evaporation experiments performed in the laboratory, that an unambiguous ^{13}C-enrichment occurs with an increase of aridity factor, i.e. precipitation:evaporation. Consequently, the high $\delta^{13}C_c$ values of the aquatic vertebrates from Buxières-les-Mines and the Muse OSB could be related to extensive drying events occurring in an arid environment. This is congruent with the interpretation of the $\delta^{18}O_p$ values.

$\delta^{13}C_c$ of temnospondyls are lower than those of strict aquatic taxa, with an average of –2.6‰ with low variability (sd = 0.1). Again, these values could be interpreted as ecological partitioning but not due to their semi-terrestrial way of life. In fact, during the late Palaeozoic (e.g. Davies et al., 2012), the marine organic matter had lower $\delta^{13}C$ values than the terrestrial one, contrary to the present day (e.g. Clementz and Koch, 2001). The observed difference between the temnospondyls and the aquatic vertebrates, ranging from 2‰ to 5‰, could be caused by different life habits. As the high $\delta^{13}C_c$ values of aquatic vertebrates are evidence for an arid environment linked to extensive water evaporation, the lower $\delta^{13}C_c$ values of temnospondyls could reflect an opposite process. When the palaeo-lake in Buxières-les-Mines experienced arid conditions, temnospondyls could be able to move to more humid environments being less influenced by water evaporation, like a humid forest. This is congruent with modern amphibians that avoid arid environments (Zancolli et al., 2014) and the ecological hypothesis of $\delta^{18}O_p$ values that postulated a life partly in a tropical humid forest for the temnospondyls of Buxières-les-Mines.

453 *5.2.4. Reconstruction of palaeotemperatures*

454 Water palaeotemperatures were calculated using the phosphate-water temperature
455 equation of Lécuyer et al. (2013), and using the $\delta^{18}O_w$ values of five different modern aquatic
456 environments as possible analogues to those of the Muse OSB and Buxières-les-Mines where
457 the vertebrates lived (Fig. 10; see Table S2 for detailed values): seawater with (0‰) and
458 without (–1‰) glaciation (Shackleton, 1975), Lake Matano (–4.3‰; Katsev et al., 2010),
459 Lake Punta Laguna (0.93‰; Curtis et al., 1996) and Lake Tanganyika (3.85‰; Casanova and
460 Hilaire-Marcel, 1992) in order to find the most theoretically viable value.

461 For Buxières-les-Mines, the calculated palaeotemperatures (Fig. 10) range from
462 34±0.5°C to 44±0.2°C and from 29±0.5°C to 40±0.2°C for the seawater models with and
463 without glaciation respectively, from 14±0.5°C to 25±0.2°C for the Lake Matano model, from
464 38±0.5°C to 48±0.2°C for the Lake Punta Laguna model and from 52±0.5°C to 62±0.2°C for
465 the Lake Tanganyika model. For the Muse OSB, the palaeotemperatures (Fig. 10) range from
466 9±5°C to 38.1±0.1°C and from 5±5°C to 33.6±0.1°C for the seawater models with and
467 without glaciation respectively, from –10±5°C to 18.8±0.1°C for the Lake Matano model,
468 from 13±5°C to 42.3±0.1°C for the Lake Punta Laguna model and from 27±5°C to
469 55.9±0.1°C for the Lake Tanganyika model.

470 The viable environmental temperatures of extant tropical actinopterygians range from
471 16°C to 40°C (Pandian and Vivekanandan, 1985) and those of freshwater stingrays from 25°C
472 to 33°C (Almeida et al., 2009). According to these viable modern temperature ranges, the
473 most viable palaeotemperature model, i.e. with temperatures between 14.4°C to 24.8°C (Fig.
474 10; Table S2), for Buxières-les-Mine is the Lake Matano, a tropical freshwater lake with a
475 significant depth (several hundred meters). The water budget of the Lake Matano is triggered
476 by a monsoon regime, i.e. with an alternation of dry and wet seasons. Moreover, aridity
477 events have been proposed at Buxières-les-Mines based on sedimentological facies analyses

(Kaulfuß, 2003). According to this body of knowledge, this Permian locality, as already supposed, could have been a rather deep tropical palaeo-lake. This hypothetical aquatic palaeoenvironment is also compatible with the documented faunal association extending from small actinopterygians to large *Orthacanthus*, as well as temnospondyls (e.g. Steyer et al., 2000). It is worth to note that such faunal diversity could not be present in small hydrological systems because it would require a large aquatic environment like open lakes to develop and to remain steady (Salzburger et al., 2014).

For the Muse OSB, the lowest $\delta^{18}O_p$ values agrees with viable temperature (Fig. 10) in a model similar to the Lake Punta Laguna model which is a shallow freshwater lake with only a few meters depth, so a good analogue to the coastal freshwater lake proposed by Mercuzot (2020) and Mercuzot et al. (2022). The presence of only small-sized animals supports the hypothesis of a shallow environment.

5.3. Palaeoecology of xenacanths and acanthodians

Along the *Orthacanthus* dorsal spine, $\delta^{13}C_c$ values vary cyclically (Fig. 4). The apparent cycles whose amplitude does not exceed 1‰ could correspond to changes in the water budget of the lake. However, the sole investigated cf. *Triodus* sp. (D08) shows a clear decrease in the $\delta^{13}C_c$ values (3‰) from the apex to the base. The $\delta^{13}C_c$ decrease is positively correlated to the $\delta^{18}O_p$ values in the same specimen (see Table S1). It has been demonstrated that a $\delta^{13}C$–$\delta^{18}O$ covariation can occur in closed-basin lakes (e.g. Li and Ku, 1997; Horton et al., 2015). Following our palaeoenvironmental reconstruction, Buxières-les-Mines therefore is interpreted as a closed-basin lake and the co-variation in $\delta^{13}C_c$ and $\delta^{18}O_p$ values could be related to changes in the water level. Here, the decrease from the apex to the base could indicate that specimen D08 moved from a shallow environment to a deeper setting during its

lifespan, as it grew. This could be related to habitat partitioning between juveniles (shallow environment) and adults (deeper environment) as in modern sharks (DeAngelis et al., 2008).

The variation in the $\delta^{18}O_p$ values along the acanthodian spines from Buxières-les-Mines (Fig. 6) does not exceed more than 0.5‰, which could correspond to known temperature variations, i.e. up to 2°C, in modern tropical lakes (Lewis Jr, 1987). Consequently, the living environment of acanthodians seems to have remained quite the same all along their lifes.

Similar conclusions are inferred from the xenacanths from Buxières-les-Mines with $\delta^{18}O_p$ variations that also do not exceed 1‰ (Fig. 3C). However, the variation pattern differs to that of acanthodians. In four specimens, a distinct decrease is reported and reach up to 1.5‰ in specimen D11. As the observed values are lower than 22%, they could be related to changes in water supply caused by wet and dry seasons as already proposed for this locality (Kaulfuß, 2003).

The $\delta^{18}O_p$ variation along the acanthodians fin spines from Muse OSB is negligible (sd=0.1) for one spine (1955) and more variable in another one (1924) with a significant decrease from the apex to the base. Spine 1955 has values ranging from 19‰ to 20‰, while those of spine 1924 vary from 20‰ to more than 21‰. These $\delta^{18}O_p$ values show that the acanthodians could live in variable environments and were able to endure drying periods. A $\delta^{13}C$–$\delta^{18}O$ covariation is observed in specimen 1924 (see Table S1) as observed in xenacanths from Buxières-les-Mines. The $\delta^{13}C$ and $\delta^{18}O$ values decrease in the same way from the apex to the base, suggesting once again changes in the hydrological budget.

This ability to live in a shallow low-oxygenised environment was already proposed for xenacanthiforms based on morphological arguments (e.g. Compagno, 1990). In the Muse OSB, the dorsal spines with the most variable $\delta^{18}O_p$ values are also those with the highest $\delta^{18}O_p$ values (Fig. 3A). This could be evidence for the ability of xenacanthiforms to live in

shallow freshwater environments submitted to high hydrological variations like periods of drying. This interpretation follows Mercuzot's (2020) and Mercuzot et al.'s (2022) conclusions in considering Muse OSB as a shallow and coastal lake, i.e. with a depth of only a few meters.

The variations in $\delta^{34}S$ continuously decrease in the investigated cf. *Acanthodes* sp. and cf. *Triodus* sp. specimens, contrary to what is observed in cf. *Orthacanthus* sp (Fig. 5). The $\delta^{34}S$ value of the environmental water vary in response to changes in river runoff ($\delta^{34}S$ = 0–10%; Krouse, 1980), volcanic inputs ($\delta^{34}S \approx 0\%$; Paytan et al., 2020), and deposition of evaporite minerals ($\delta^{34}S \approx 21\%$) or sedimentary iron sulfides such as pyrite ($\delta^{34}S$ = –15%; Krouse, 1980; Kaplan, 1983). Buxières-les-Mines and the Muse OSB could have been two intra-mountainous lacustrine systems submitted to intense river runoff due to their palaeogeographical location in the Hercynian Mountains. Moreover, the basins of the French Massif central were exposed to a recurrent volcanic activity as attested by the presence of tonsteins and ash levels documented in the sedimentary deposits of the two studied localities (e.g. Steyer et al., 2000; Pellenard et al., 2017). Consequently, the observed $\delta^{34}S$ variation within the xenacanth and acanthodian spines could reflect a combination of such environmental fluctuations.

5.4. Trophic and food web

Considering that the $\delta^{13}C_c$ values reflect those of organic matter before the mineralization process in the vertebrate skeleton, the $\delta^{13}C_c$ of predators is expected to be higher by almost 1‰ relative to their potential preys (e.g. Cerling and Harris 1999). This pattern of isotopic enrichment within the trophic chain could be indeed recorded in the $\delta^{13}C_c$ of acanthodians, actinopterygians and the small xenacanthid *Triodus.* It is therefore surprising that the large diplodoselachid *Orthacanthus* has such low $\delta^{13}C_c$ values (from –0.4‰ to 1.9‰).

552 Boy and Schindler (2000) and Kriwet et al. (2008) proposed that the large *Orthacanthus* was
553 the apex predator of its ecosystem, feeding on all the other smaller predators such as *Triodus*
554 and temnospondyls. Indirect evidence of consumption of *Triodus* by *Orthacanthus* in the
555 Puertollano Basin (Gzhelian of Spain) was reported by Soler-Gijón (1995) and temnospondyl
556 mandible with an *Orthacanthus* tooth stuck in it was reported from Buxières-les-Mines (Fig.
557 11). It is therefore probable that, in Buxières-les-Mines, *Orthacanthus* preyed on *Triodus* and
558 temnospondyls too. The *Orthacanthus* $\delta^{13}C_c$ values are intermediate between those of *Triodus*
559 and temnospondyls. If *Orthacanthus* preyed on these two taxa, these values are expected
560 because they reflect the diversity of its preys: *Triodus* evolving in strict aquatic environments
561 and temnospondyls evolving in a semi-terrestrial one.
562 The faunal composition of the investigated localities is compatible with the two
563 proposed environmental interpretations (Fig. 12). In Buxières-les-Mines, many components of
564 the Carboniferous-Permian freshwater fauna were already reported in other basins like the
565 Saar-Nahe Basin and its large lacustrine system (e.g. Kriwet et al., 2008). These observations
566 favour the hypothesis of an open, large and deep lake, in which the complete food web is
567 represented with large predators or tertiary consumers (*Orthacanthus* and temnospondyls),
568 small predators or secondary consumers (*Triodus*) and preys as well as small consumers or
569 primary consumers (acanthodians and actinopterygians). In the Muse OSB, the food web is
570 mainly limited to small consumers (acanthodians and actinopterygians) and small predators
571 (*Triodus*). A systematic revision has shown that a large *Orthacanthus* was present in the Muse
572 OSB with *O.* cf. *kounoviensis* (Luccisano et al., 2022). The single reported lateral tooth does
573 not reach the size of the large adult teeth of *O. kounoviensis* from Buxières-les-Mines, so it
574 could correspond to a medium-sized animal distinct from the very large *Orthacanthus*
575 recovered from Buxières-les-Mines, or to a late juvenile or a sub-adult specimen.
576 Consequently, this shark could have been able to live in shallow as well as large lakes.

However, the presence of this single tooth in the Muse OSB could be questioned because its stratigraphic origin is unclear. Even if it is supposed to come from the base of the Muse OSB (Luccisano et al., 2022), no *Orthacanthus* material was found during recent excavation campaigns (Gand et al., 2011, 2015; and during the last campaign in 2021). As the Muse OSB presents a distinct East-oriented dip and the provenance of the tooth is unclear according to Heyler (1969), this tooth could come from a different stratigraphic level older or younger than the analysed material. In the light of our results, the Muse OSB fauna is more likely to be related to a small and shallow aquatic environment than to open and large lakes or river-channels.

5.5. Implication for the palaeobiogeography of the xenacanths at the Carboniferous-Permian transition

Our analyses also show a differential environmental adaptiveness among the Xenacanthiformes of the Early Permian. The large Diplodoselachidae were restricted to large and deep lakes and river systems like Buxières-les-Mines in France whereas the small Xenacanthidae were able to inhabit more diversified environments, ranging from large lakes to shallow swamps like in the Muse OSB. The observed different ecologies fit in with the current known palaeobiogeography of the Carboniferous-Permian Xenacanthiformes from Europe. The large xenacanthiforms like *Orthacanthus* are almost restricted to the upper Carboniferous in which large freshwater basins in connection with each other were present (e.g. Luccisano et al., 2022). At the Carboniferous-Permian transition, the Francovian tectonic motions suppressed the connections between large basins containing large and deep lakes like Buxières-les-Mines (e.g. Schneider, 1996). The resulting isolated basins were of smaller size and contained smaller lacustrine systems like the Muse OSB. In such shallow lakes, only small xenacanthiforms like *Triodus* were able to live, a scenario in compliance with the

apparent diversification of *Triodus* throughout the Early Permian. The large xenacanthiforms, however, continued to exist in a few peculiar locations such as Buxières-les-Mines or the Saar-Nahe Basin, in which large and deep lakes prevailed.

6. Conclusions

The oxygen, carbon and sulfur isotope compositions of aquatic vertebrate bioapatite from two Early Permian localities of the French Massif central allow reconstructing their palaeoenvironment. The non-contemporaneous localities of the Muse OSB and Buxières-les-Mines accordingly represent two different aquatic environments. Buxières-les-Mines is a large, open and deep freshwater lake containing a diversified vertebrate fauna, ranging from large xenacanthiforms to small actinopterygians. *A contrario*, the Muse OSB is a less taxonomically diversified locality with only small sized vertebrates that lived in a shallow freshwater environment experienced periodic and intense drying events. These localities illustrate the environmental changes of the aquatic setting of the Early Permian intra-mountainous basins of the European Hercynian Mountains. Buxières-les-Mines is a remnant of the large lacustrine systems of the upper Carboniferous, in which diversified aquatic vertebrates occurred. It represents one of the last large lacustrine systems in the Early Permian of Europe. The Muse OSB represents one of the most common intra-mountainous freshwater ecosystems occurring during the Early Permian. It contains a less diversified fauna than in Buxières-les-Mines with vertebrates small in size evolving in shallow lakes or swamps, most likely cyclically submitted to significant drying up events. This study also agrees with previous analyses that postulated that these intra-mountainous basins were not submitted to a significant marine influence during the Early Permian.

This palaeoenvironmental reconstruction revealed that Early Permian Xenacanthiformes from France lived in a rather uniform freshwater environment with no or restricted marine influences and without migrations into marine settings. However, small

xenacanthiforms were adapted to extreme conditions such as drying events or low oxygenated waters. This adaptation could explain their diversification in the Early Permian. These palaeoecological assumptions are contrary to those previously deduced from American species. Further studies conducted at regional or global scales will be able to identify different adaptive strategies within this group during their evolutionary history and to explain their global distribution in the Late Palaeozoic.

Acknowledgements

The authors thank the Rhinopolis Association, the Buxières-les-Mines Town hall and the Conseil Départemental de l'Allier for the funding of the excavation campaigns in Buxières-les-Mines during which the studied specimens were recovered, and for providing storage space in which the Buxières-les-Mines fossils are housed. They also thank the Muséum d'Histoire Naturel d'Autun (MHNA) and its curator Dominique Chabard for access to the Muse OSB specimens. Specimens from the Muse OSB were found during several excavation campaigns (2010-2014 and 2021) and the authors thank for their valuable help D. Beaudoin, F. Beaudoin, R. Pillon, G. Barnay, P. Baudinaud, N. Pégon, B. Arnoult (SHNA), D. Chabard, E. Chabard, A. Margueron (MHNA), the Gevrey, Barnay, and Jacquemard families, G. Grillot, S. Kunz (Dracy-Saint-Loup Municipality) B. Blanc (Marine), E. Chenal (Éducation Nationale), C. Delhaye (CNRS), I. van Waveren and her students (Naturalis, Leiden), J. Fortuny (ICP, Barcelona), S. Hervet (PaléOvergne), J. Galtier (Montpellier), A. Bercovici (Manchester University), F. Prost (Dijon University), S. Giner (Var Département), K. Rey (ex-BPI), and J.-S. Steyer, O. Béthoux, G. Cousin, G. Odin, L. Anseaume, J. Barbier, M. Sanders, D. Perez, J. Falconnet, D. Germain and V. Rouchon (MNHN). All the isotopic analyses were performed at the Plateforme d'Écologie Isotopique of UMR 5023 LEHNA, Université Claude Bernard Lyon 1, France, member of the RéGEF network. The first author

was funded by the Doctoral School ED 341 - E2M2 Évolution Écosystème Microbiologie Modélisation, Université Claude Bernard Lyon 1, France.

Authorship contribution statement

V. L., G.C., A.P., R.A. and C. L. designed the research. V.L., K. L., R. A. and F.F. performed the analyses. V.L. wrote the original draft and prepared the figures and tables. J.-M.P. made the material available and led the field work in Buxières-les-Mines. All authors discussed, wrote and approved the manuscript.

Data availability

All data are available in the supplementary materials and within the present article.

Declaration of competing interest

The authors declare no conflict of interest.

References

Almeida, M.P.D., Barthem, R.B., Viana, A.D.S., Charvet-Almeida, P., 2009. Factors affecting the distribution and abundance of freshwater stingrays (Chondrichthyes: Potamotrygonidae) at Marajó Island, mouth of the Amazon River. Pan-Am. J. Aquat. Sci. 4, 1–11.

Amiot, R., Wang, X., Lécuyer, C., Buffetaut, E., Boudad, L., Cavin, L., Ding, Z., Fluteau, F., Kellner, A.W.A., Tong, H., Zhang, F., 2010. Oxygen and carbon isotope compositions of middle Cretaceous vertebrates from North Africa and Brazil: ecological and environmental significance. Palaeogeogr. Palaeoclimatol. Palaeoecol. 297, 439–451.

Beck, K.G., Soler-Gijón, R., Carlucci, J.R., Willis, R.E., 2016. Morphology and histology of dorsal spines of the xenacanthid shark *Orthacanthus platypternus* from the Lower

679 Permian of Texas, USA: Palaeobiological and palaeoenvironmental implications. Acta
680 Palaeontol. Pol. 61, 97–117.
681 Błażejowski, B., Duffin, C.J., Gieszcz, P., Małkowski, K., Binkowski, M., Walczak, M.,
682 Mcdonald, A.A., Withers, P.J., 2013. *Saurichthys* (Pisces, Actinopterygii) teeth from
683 the Lower Triassic of Spitsbergen, with comments on their stable isotope composition
684 ($\delta^{13}C$ and $\delta^{18}O$) and X-ray microtomography. Pol. Polar Res. 34, 23–38.
685 Boy, J.A., Schindler, T., 2000. Ökostratigraphische Bioevents im Grenzbereich
686 Stephanium/Autunium (höchstes Karbon) des Saar-Nahe-Beckens (SW-Deutchland)
687 und benachbarter Gebiete. Neues. Jahrb. Geol. Palaontol. Abh. 216, 89–152.
688 Brudefold, F., Soremark, R., 1967. Chapter 18 Chemistry of the mineral phase of enamel. in:
689 Miles, A.E.W. (Ed.), Structural and Chemical Organization of Teeth. Academic Press
690 Inc, New York, pp. 247–277.
691 Bryant, J.D., Froelich, P.N., Showers, W.J., Genna, B.J., 1996. Biologic and climatic signals
692 in the oxygen isotopic composition of Eocene-Oligocene equid enamel phosphate.
693 Palaeogeogr, Palaeoclimatol, Palaeoecol. 126, 75–8.
694 Burrow, C.J., den Blaauwen, J., Newman, M., Davidson, R., 2016. The diplacanthid fishes
695 (Acanthodii, Diplacanthiformes, Diplacanthidae) from the Middle Devonian of
696 Scotland. Palaeontol. Electron. 19, 1–83.
697 Burrow, C.J., Davidson, R.G., Den Blaauwen, J.L., Newman, M.J., 2015. Revision of
698 *Climatius reticulatus* Agassiz, 1844 (Acanthodii, Climatiidae), from the Lower
699 Devonian of Scotland, based on new histological and morphological data. J. Vertebr.
700 Paleontol. 35, e913421.
701 Carey, F. G., Teal, J. M., 1969. Regulation of body temperature by the bluefin tuna. Comp.
702 Biochem. Physiol. 28, 205–213.

703 Carpenter, D., Falcon-Lang, H.J., Benton, M.J., Nelson, J.W., 2011. Fishes and tetrapods in
704 the Upper Pennsylvanian (Kasimovian) Cohn coal member of the Mattoon formation
705 of Illinois, United States: systematics, paleoecology, and paleoenvironments. Palaios.
706 26, 619–657.
707 Casanova, J., Hilaire-Marcel, C., 1992. Late Holocene hydrological history of Lake
708 Tanganyika, East Africa, from isotopic data on fossil stromatolites. Palaeogeogr,
709 Palaeoclimatol, Palaeoecol. 91, 35–48.
710 Cerling, T.E., Harris, J.M., 1999. Carbon isotope fractionation between diet and bioapatite in
711 ungulate mammals and implications for ecological and paleoecological studies.
712 Oecologia. 120, 347–363.
713 Châteauneuf, J.J., 1980. Synthèse géologique des bassins permiens français. Mém. BRGM.
714 82, 1–124.
715 Châteauneuf, J.J., Farjanel, G., 1989. Synthèse géologique des bassins permiens français.
716 Mém. BRGM. 1–128.
717 Châteauneuf, J.J., Farjanel, G., Pacaud, G., Broutin, J., 1992. The Autun permian basin, the
718 autunian startotype. Cah. Micropaléontol. 7, 123–139.
719 Chen, B., Joachimski, M.M., Shen, S.-Z., Lambert, L.L., Lai, X.L., Wang, X.-D., Chen, J.,
720 Yuan, D.X., 2013. Permian ice volume and palaeoclimate history: Oxygen isotope
721 proxies revisited. Gondwana Res. 24, 77–89.
722 Claypool, G.E., Holser, W.T., Kaplan, I.R., Sakai, H., Zak, I., 1980. The age curves of sulfur
723 and oxygen isotopes in marine sulfate and their mutual interpretation. Chem. Geol. 28,
724 199–260.
725 Clementz, M.T., Koch, K.L., 2001. Differentiating aquatic mammal habitat and foraging
726 ecology with stable isotopes in tooth enamel. Oecologia. 129, 461–472.

727 Compagno, L.J.V., 1990. Alternative life-history styles of cartilaginous fishes in time and
728 space. Environ. Biol. Fishes. 28, 33–75.
729 Coplen, T.B., Brand, W.A., Gehre, M., Gröning, M., Meijer, H.A.J., Toman, B., Verkouteren,
730 R.M., 2006. New guidelines for ^{13}C measurements, Anal. Chem. 78, 2439–2441.
731 Crowson, R.A., Showers, W.J., Wright, E.K., Hoering, T.C., 1991. Preparation of Phosphate
732 Samples for Oxygen Isotope Analysis. Anal. Chem. 63, 2397–2400.
733 Curtis, J.H., Hodell, D.A., Brenner, M., 1996. Climate variability on the Yucatan Peninsula
734 (Mexico) during the past 3500 years, and implications for Maya cultural evolution.
735 Quat. Res. 46, 37–47.
736 Dansgaard, W., 1964. Stable isotopes in precipitation. Tellus. 16, 436–468.
737 Davies, S.J., Leng, M.J., Macquaker, J.H.S., Hawkins, K., 2012. Sedimentary process control
738 on carbon isotope composition of sedimentary organic matter in an ancient shallow-
739 water shelf succession. Geochem. Geophys. Geosystems. 13, Q0AI04.
740 DeAngelis, B.M., McCandless, C.T., Kohler, N.E., Recksiek, C.W., Skomal, G.B., 2008. First
741 characterization of shark nursery habitat in the United States Virgin Islands: evidence
742 of habitat partitioning by two shark species. Mar. Ecol. Prog. 358, 257–271.
743 Debriette, P., 1992. Le bassin de Bourbon-l'Archambault et le sillon houillier (Allier, France).
744 Présentation et itinéraire géologique. Bulletin Trimestriel de la Société d'Histoire
745 Naturelle des Amis du Muséum d'Autun. 144, 13–34.
746 Ducassou, C., Bourquin, S., Pellenard, P., Beccaletto, L., Mercuzot, M., Rossignol, C.,
747 Poujol, M., Hallot, E., Pierson-Wickmann, A.-C., Gand, G., 2018. Caractérisation
748 pétro-géochimique et datation U/Pb du volcanisme contemporain des bassins d'âge
749 fini-Carbonifère à Permien du Nord du Massif Central. 26ème Réunion des Sciences
750 de la Terre, Lille.

751 Fischer, J., Schneider, J.W., Voigt, S., Joachimski, M.M., Tichomirowa, M., Tütken, T.,
752 Götze, J., Berner, U., 2013. Oxygen and strontium isotopes from fossil shark teeth:
753 Environmental and ecological implications for Late Palaeozoic European basin. Chem.
754 Geol. 342, 44–62.
755 Fischer, J., Schneider, J.W., Hodnett, J.-P.M., Elliott, D.K., Johnson, G.D., Voigt, S.,
756 Joachimski, M.M., Tichomirowa, M., Götze, J., 2014. Stable and radiogenic isotope
757 analyses on shark teeth from the Early to the Middle Permian (Sakmarian–Roadian) of
758 the southwestern USA. Hist. Biol. 26, 710–727.
759 Fourel F., Martineau F., Seris M., Lécuyer C., 2014. Simultaneous N, C, S stable isotope
760 analyses using new purge and trap technology. Rapid Commun. Mass Spectrom. 28,
761 2587–2594.
762 Fourel F., Martineau F., Seris M., Lécuyer C., 2015. Determination of $\delta^{34}S$ of NBS120c and
763 BCR32 phosphorites using purge and trap EA–IRMS technology. Geostand. Geoanal.
764 Res. 39, 47–53.
765 Fourel, F., Martineau, F., Tóth, E.E., Görög, A., Escarguel, G., Lécuyer, C., 2016. Carbon and
766 oxygen isotope variability among foraminifera and ostracod carbonated shells. Ann.
767 UMCS sectio AAA–Physica. 70, 133.
768 Fourel, F., Martineau, F., Lécuyer, C., Kupka, H.J., Lange, L., Ojeimi, C., Seed, M., 2011.
769 $^{18}O/^{16}O$ ratio measurements of inorganic and organic materials by elemental analysis–
770 pyrolysis–isotope ratio mass spectrometry continuous-flow technique. Rapid Com.
771 Mass Spectrom. 25, 2691–2696.
772 Fricke, H.C., Clyde, W.C., O'Neil, J.R., Gingerich, P.D., 1998. Evidence for rapid climate
773 change in North America during the latest Paleocene thermal maximum: oxygen
774 isotope compositions of biogenic phosphate from the Bighorn Basin
775 (Wyoming). Earth Planet. Sci. Lett. 160, 193–208.

776 Friedman, I., O'Neil, J., Cebula, G., 1982. Two new carbonate stable isotope standards.
777 Geostand. newsl. 6, 11–12.
778 Gand, G., Steyer, J.-S., Chabard, D., 2011. Reprise de fouilles paléontologiques dans un gîte
779 bourgignon célèbre : les “schistes bitumineux” de l’Autunien de Muse (Bassin
780 d’Autun) Bilan 2010 et perspectives. Bourgogne-Franche-Comté Nature. 12, 10–29.
781 Gand, G., Pellenard, P., Galtier, J., Broutin, J., Steyer, J.-S., 2017. Le stratotype autunien du
782 bassin d’Autun (Bourgogne-France) : évolution de la stratigraphie et des âges. Bulletin
783 Trimestriel de la Société d’Histoire Naturelle des Amis du Muséum d’Autun. 211, 19–
784 36.
785 Gand, G., Steyer, J.S., Pellenard, P., Béthoux, O., Odin, G., Rouchon, V., Van Waveren, I., de
786 Ploeg, G., Chabard, D., 2015. Le stratotype autunien (Permien) du bassin d’Autun:
787 résultats préliminaires des travaux réalisés en 2014 sur les niveaux de la couche de
788 Muse (Saône-et-Loire, France). Bulletin Trimestriel de la Société d’Histoire Naturelle
789 des Amis du Muséum d’Autun. 207, 12–31.
790 Gang, L., Baorong, G., Ermi, Z., 2004. *Andrias davidianus*. The IUCN Red List of
791 Threatened Species e.T1272A3375181.
792 Ginter, M., Hampe, O., Duffin, C.J., 2010. Handbook of Paleoichthylology - Volume 3D-
793 Chondrichtyes - Paleozoic Elasmobranchii: Teeth, Schultze, H.-P., Kuhn, O. (Eds.),
794 Verlag Dr. Friedrich Pfeil, Munich, 168 pp.
795 Goedert, J., 2017. Écologie des premiers tétrapodes dévoilée par la composition isotopique du
796 soufre ($^{34}S/^{32}S$) de leurs squelettes. Unpublished Ph. D. thesis, Université Claude
797 Bernard Lyon 1, Villeurbanne, 239 pp.
798 Goedert, J., Fourel, F., Amiot, R., Simon, L., Lécuyer, C., 2016. High-precision $^{34}S/^{32}S$
799 measurements in vertebrate bioapatites using purge-and-trap elemental

analyser/isotope ratio mass spectrometry technology. Rapid Commun. Mass Spectrom. 30, 2002–2008.

Goedert, J., Amiot, R., Berthet, D., Fourel, F., Simon, L., Lécuyer, C., 2020. Combined oxygen and sulphur isotope analysis—a new tool to unravel vertebrate (paleo)-ecology. Sci. Nat. 107, 1–9.

Goedert, J., Lécuyer, C., Amiot, R., Arnaud-Godet, F., Wang, X., Cui, L., Cuny, G., Douay, G., Fourel, F., Panczer, G., Simon, L., Steyer, J.-S., Zhu, M., 2018. Euryhaline ecology of early tetrapods revealed by stable isotopes. Nature. 558, 68–72.

Goldman, K. J., 1997. Regulation of body temperature in the white shark, *Carcharodon carcharias*. J. Comp. Physiol. B. 167, 423–429.

Haesemeyer, M., 2020. Thermoregulation in fish. Mol. Cell. Endocrinol. 518, 110986.

Halas, S., Szaran, J., 2001. Improved thermal decomposition of sulfates to SO_2 and mass spectrometric determination of $\delta^{34}S$ of IAEA SO-5, IAEA SO-6 and NBS-127 sulfate standards. Rapid Commun. Mass Spectrom. 15, 1618–1620.

Halas, S., Skrzypek, G., Meier-Augenstein, W., Pelc, A., Kemp, H.F., 2011. Inter-laboratory calibration of new silver orthophosphate comparison materials for the stable oxygen isotope analysis of phosphates. Rapid Commun. Mass Spectrom. 25, 579–584.

Hampe, O., 2003. Revision of the Xenacanthida (Chondrichthyes: Elasmobranchii) from the Carboniferous of the British Isles. Earth Environ. Sci. Trans. R. Soc. Edinb. 93, 191–237.

Hampe, O., Johnson, G.D., Turner, S., 2006. *Dicentrodus* (Chondrichthyes: Xenacanthida) from the Early Carboniferous (Visean: upper St Louis Formation) of Iowa, USA. Geol. Mag. 143, 545–549.

Heyler, D., 1969. Vertébrés de l'Autunien de France, Centre National de la Recherche Scientifique, Paris, 259 pp.

825 Horton, T.W., Defliese, W.F., Tripati, A.K., Oze, C., 2015. Evaporation induced ^{18}O and ^{13}C
826 enrichment in lake systems: A global perspective on hydrologic balance effects. Quat.
827 Sci. Rev. 131, 365–379.
828 Hut, G., 1987. Stable Isotope Reference Samples for Geochemical and Hydrological
829 Investigations, International Atomic Energy Agency, Vienna, 42 pp.
830 Iacumin, P., Bocherens, H., Mariotti, A., Longinelli, A., 1996. Oxygen isotope analyses of co-
831 existing carbonate and phosphate in biogenic apatite: a way to monitor diagenetic
832 alteration of bone phosphate? Earth Planet. Sci. Lett. 142, 1–6.
833 Jerve, A., Bremer, O., Sanchez, S., Ahlberg, P.E., 2017. Morphology and histology of
834 acanthodian fin spines from the late Silurian Ramsåsa E locality, Skåne, Sweden.
835 Palaeontol. Electron. 20.3.56A, 1–19.
836 Joachimski, M.M., von Bitter, P.H., Buggisch, W., 2006. Constraints on Pennsylvanian
837 glacioeustatic sea-level changes using oxygen isotopes of conodont apatite. Geology.
838 34, 277–280.
839 Joachimski, M.M., Van Geldern, R., Breisig, S., Buggisch, W., Day, J., 2004. Oxygen isotope
840 evolution of biogenic calcite and apatite during the Middle and Late Devonian. Int. J.
841 Earth Sci. 93, 542–553.
842 Joachimski, M.M., Breisig, S., Buggisch, W., Talent, J.A., Mawson, R., Gereke, M., Morrow,
843 J.R., Day, J., Weddige, K., 2009. Devonian climate and reef evolution: insights from
844 oxygen isotopes in apatite. Earth Planet. Sci. Lett. 284, 599–609.
845 Johnson, G.D., 1999. Dentitions of Late Palaeozoic *Orthacanthus* species and new species
846 of ?*Xenacanthus* (Chondrichthyes: Xenacanthiformes) from North America. Acta
847 Geol. Pol. 49, 215–266.
848 Kaplan, I.R., 1983. Stable isotopes of sulfur, nitrogen and deuterium in recent marine
849 environments, in: Arthur, M.A., Anderson, T.F., Kaplan, I.R., Veizer, J., Land, L.S.,

(Eds.), Stable Isotopes in Sedimentary Geology. Society of Economic Paleontologists and Mineralogists Short Course, Dallas, pp. 2.1–2.108.

Katsev, S., Crowe, S.A., Mucci, A., Sundby, B., Nomosatryo, S., Haffner, D.G., Fowlef, D.A., 2010. Mixing and its effects on biogeochemistry in the persistently stratified, deep, tropical Lake Matano, Indonesia. Limnol. Oceanogr. 55, 763–776.

Kaulfuß, U., 2003. Lithofazies, Genese und Stratigraphie des Permokarbon im Becken von Bourbon-l`Archambault (Massif central) – Fallstudie Buxières-les-Mines. Unpublished Master thesis, Bergakademie Freiberg Technische Universität, Freiberg, 82 pp.

Koch, P.L., Tuross, N., Fogel, M.L., 1997. The Effects of Sample Treatment and Diagenesis on the Isotopic Integrity of Carbonate in Biogenic Hydroxylapatite. J. Archaeol. Sci. 24, 417–429.

Kolodny, Y., Luz, B., 1991. The isotopic record of oxygen in phosphates of fossil fish-Devonian to Recent, in: Taylor, H.P. Jr., O'Neil, R., Kaplan, I.R. (Eds.), Stable isotope geochemistry: A tribute to Samuel Epstein. The Geochemical Society, Special Publication, Alexandria, pp. 105–119.

Kolodny, Y., Luz, B., Navon, O., 1983. Oxygen isotope variations in phosphate of biogenic apatites, I. Fish bone apatite—rechecking the rules of the game. Earth Planet. Sci. Lett. 64, 398–404.

Kriwet, J., Witzmann, F., Klug, S., Heidtke, U.H.J., 2008. First direct evidence of a vertebrate three-level trophic chain in the fossil record. Proc. Royal Soc. B. 275, 181–186.

Krouse, H.R. 1980. Sulphur isotopes in our environment, in: Fritz, P., Fontes, J.C. (Eds.), Isotope Geochemistry, Vol. 1. The Terrestrial Environment. Elsevier, Amsterdam, pp. 435–71.

874 Kutzbach, J.E., Ziegler, A.M., 1994. Simulation of Late Permian climate and biomes with an
875 atmosphere-ocean model: comparisons with observations. Philos. Trans. R. Soc.
876 Lond., B, Biol. Sci. 341, 327–340.
877 Laurin, M., Soler-Gijón, R., 2010. Osmotic tolerance and habitat of early stegocephalians:
878 indirect evidence from parsimony, taphonomy, palaeobiogeography, physiology and
879 morphology. Geol. Soc. Spec. Publ. 339, 151–179.
880 Lécuyer, C., Amiot, R., Touzeau, A., Trotter, J., 2013. Calibration of the phosphate $\delta^{18}O$
881 thermometer with carbonate–water oxygen isotope fractionation equations. Chem.
882 Geol. 347, 217–226.
883 Lécuyer, C., Grandjean, P., O'Neil, J.R., Cappetta, H., Martineau, F., 1993. Thermal
884 excursions in the ocean at the Cretaceous-Tertiary boundary (northern Morocco): $\delta^{18}O$
885 record of phosphatic fish debris. Palaeogeogr, Palaeoclimatol, Palaeoecol. 105, 235–
886 243.
887 Lécuyer, C., Bogey, C., Garcia, J.P., Grandjean, P., Barrat, J.A., Floquet, M., Bardet, N.,
888 Pereda-Superbiola, X., 2003. Stable isotope composition and rare earth element
889 content of vertebrate remains from the Late Cretaceous of northern Spain (Laño): did
890 the environmental record survive? Palaeogeogr, Palaeoclimatol, Palaeoecol. 193, 457–
891 471.
892 Lewis Jr, W.M., 1987. Tropical limnology. Annu. Rev. Ecol. Syst. 18, 159–184.
893 Li, H.C., Ku, T.L., 1997. $\delta^{13}C$–$\delta^{18}C$ covariance as a paleohydrological indicator for closed-
894 basin lakes. Palaeogeogr, Palaeoclimatol, Palaeoecol. 133, 69–80.
895 Luccisano, V., Pradel, A., Amiot, R., Gand, G., Steyer, J. S., & Cuny, G., 2021. A new
896 *Triodus* shark species (Xenacanthidae, Xenacanthiformes) from the lowermost
897 Permian of France and its paleobiogeographic implications. J Vertebr Paleontol. 41,
898 e1926470.

899 Luccisano, V., Pradel, A., Amiot, R., Pouillon, J. M., Kindlimann, R., Steyer, J.-S., Cuny, G.,
900 2022. Systematics, ontogeny and palaeobiogeography of the genus *Orthacanthus*
901 (Diplodoselachidae, Xenacanthiformes) from the lower Permian of France. Pap.
902 Palaeontol. 8, e1470.
903 Maisey, J.G., 1978. Growth and Form of finspines in Hybodont sharks. Palaeontology. 21,
904 657–666.
905 Maisey, J.G., 1979. Finspine morphogenesis in squalid and heterodontid sharks. Zool. J. Linn.
906 Soc. 66, 161–183.
907 Maisey, J.G., 1982. Studies on the Paleozoic selachian genus *Ctenacanthus* Agassiz. No. 2,
908 *Bythiacanthus* St. John and Worthen, *Amelacanthus*, new genus, *Eunemacanthus* St.
909 John and Worthen, *Sphenacanthus* Agassiz, and Wodnika Münster. Am. Mus. Novit.
910 2722, 1–24.
911 Marteau, P., 1983. Le bassin permo carbonifère d'Autun: stratigraphie, sédimentologie et
912 aspects structuraux. Unpublished Ph.D. Thesis, Université de Dijon, Dijon, 183 pp.
913 McConnaughey, T. A., Burdett, J., Whelan, J. F., & Paull, C. K., 1997. Carbon isotopes in
914 biological carbonates: respiration and photosynthesis. Geochim. Cosmochim.
915 Acta. 61, 611–622.
916 Mercuzot, M., 2020. Reconstitutions paléoenvironnementales et paléoclimatiques en contexte
917 tardi-orogénique : cas des bassins fini carbonifères à permiens du nord-est du Massif
918 central, France. Unpublished Ph.D. Thesis, Université de Rennes 1, Rennes, 551 pp.
919 Mercuzot, M., Bourquin, S., Pellenard, P., Beccaletto, L., Schnyder, J., Baudin, F., Ducassou,
920 C., Garel, S., Gand, G., 2022. Reconsidering Carboniferous–Permian continental
921 paleoenvironments in eastern equatorial Pangea: facies and sequence stratigraphy
922 investigations in the Autun Basin (France). Int. J. Earth Sci. 111, 1663–1696.

923 Nehlich, O., 2015. The application of sulphur isotope analyses in archaeological research: a
924 review. Earth Sci. Rev. 142, 1–17.
925 Olson, E.C., 1989. The Arroyo Formation (Leonardian, Lower Permian) and its vertebrate
926 fossils. T. Mem. Mus. Bull. 33, 1–25.
927 Otero, O., Lécuyer, C., Fourel, F., Martineau, F., Mackaye, H.T., Vignaud, P., Brunet, M.,
928 2010. Freshwater fish $\delta^{18}O$ indicates a Messinian change of the precipitation regime in
929 Central Africa. Geology. 39, 435–438.
930 Pandian, T.J., Vivekanandan, E., 1985. Energetics of Feeding and Digestion, in: Tytler, P.,
931 Calow, P. (Eds.), Fish Energetics. Springer, Dordrecht, pp. 99–124.
932 Paquette, Y., Doubinger, J., Courel, L., 1980. Étude palynologique de la couche du toit du
933 bassin autunien de l'Aumance (assise de Buxières): liaison avec les milieux
934 sédimentaires. Bulletin Trimestriel de la Société d'Histoire Naturelle des Amis du
935 Muséum d'Autun. 95, 85–101.
936 Parrish, J.T., 1993. Climate of the supercontinent Pangea. J. Geol. 101, 215–233.
937 Passey, B. H., Robinson, T. F., Ayliffe, L. K., Cerling, T. E., Sponheimer, M., Dearing, M.
938 D., Roeder, B. L., Ehleringer, J. R., 2005. Carbon isotope fractionation between diet,
939 breath CO_2, and bioapatite in different mammals. J. Archaeol. Sci. 32. 1459–1470.
940 Passey, B.H., Cerling, T.E., Levin, N.E., 2007. Temperature dependence of oxygen isotope
941 acid fractionation for modern and fossil tooth enamels. Rapid Commun. Mass
942 Spectrom. 21, 2853–2859.
943 Paytan, A., Yao, W., Faul, K.L., Gray, E.T., 2020. Application of sulphur isotopes for
944 stratigraphic correlation, in: Gradstein, F. M., Ogg, J.G., Schmitz, M.D., Ogg, G.M.
945 (Eds.), Geologic Time Scale 2020, Elsevier, Amsterdam, pp. 259–278.

946 Pellenard, P., Gand, G., Schmitz, M., Galtier, J., Broutin, J., Steyer, J.-S., 2017. High-
947 precision U-Pb zircon ages for explosive volcanism calibrating the NW European
948 continental Autunian stratotype. Gondwana Res. 51, 118–136.
949 Pruvost, P., 1942. Étude géologique du bassin Permo-Carbonifère d'Autun, BRGM, Orléans-
950 la-Source. 23 pp.
951 Rees, C.E., Jenkins, W.J., Monster, J. 1978. The sulphur isotopic composition of ocean water
952 sulphate. Geochim. Cosmochim. Acta. 42, 377–381.
953 Reif, W.-E., 1978. Types of morphogenesis of the dermal skeleton in fossil sharks. PalZ. 52,
954 110–128.
955 Rink, W.J., Schwarcz, H.P., 1995. Tests for diagenesis in tooth enamel: ESR dating signals
956 and carbonate contents. J. Archaeol. Sci. 22, 251–255.
957 Roscher, M., Schneider, J.W., 2006. Permo-Carboniferous climate: Early Pennsylvanian to
958 Late Permian climate development of central Europe in a regional and global context.
959 Geol. Soc. Spec. Publ. 265, 95–136.
960 Salzburger, W., Van Bocxlaer, B., Cohen, A.S., 2014. Ecology and evolution of the African
961 Great Lakes and their faunas. Annu. Rev. Ecol. Evol. Syst. 45, 519–545.
962 Santos, G. M., Ferguson, J., Acaylar, K., Johnson, K. R., Griffin, S., & Druffel, E., 2011.
963 $\Delta^{14}C$ and $\delta^{13}C$ of seawater DIC as tracers of coastal upwelling: A 5-year time series
964 from Southern California. Radiocarbon. 53, 669–677.
965 Schneider, J.W., 1996. Xenacanth teeth - a key for taxonomy and biostratigraphy. Mod. Geol.
966 20, 321–340.
967 Schneider, J.W., Werneburg, R., 2006. Insect biostratigraphy of the Euramerican continental
968 late Pennsylvanian and early Permian. Geol. Soc. Spec. Publ. 265, 325–336.

969 Schneider, J.W., Hampe, O., Soler-Gijón, R., 2000. The Late Carboniferous and Permian:
970 Aquatic vertebrate zonation in southern Spain and German basins. Cour. Forsch. Inst.
971 Senckenberg. 223, 543–561.
972 Schultze, H.-P., 1985. Marine to onshore vertebrates in the Lower Permian of Kansas and
973 their paleoenvironmental implications. Univ. Kans. Paleontol. Contrib. 113, 1–18.
974 Schultze, H.-P., 1995. Terrestrial biota in coastal marine deposits: Fossil-lagerstätten in the
975 Pennsylvanian of Kansas, USA. Palaeogeogr, Palaeoclimatol, Palaeoecol. 119, 255–
976 273.
977 Schultze, H.-P., 1998. The Fossil Record of the Intertidal Zone, in: Horn, M.H., Martin,
978 K.L.M., Chotkowski, M.A. (Eds.), Intertidal Fishes. Life in Two Worlds. Academic
979 Press, San Diego, pp. 373–392.
980 Schultze, H.-P., 2009. Interpretation of marine and freshwater paleoenvironments in Permo–
981 Carboniferous deposits. Palaeogeogr, Palaeoclimatol, Palaeoecol. 281, 126–136.
982 Schultze, H.-P., 2013. The palaeoenvironments at the transition from piscine to tetrapod
983 sarcopterygians. Bull. N. M. Mus. Nat. Hist. Sci. 60, 373–397.
984 Schultze, H.-P., Soler-Gijón, R., 2004. A xenacanth clasper from the ?uppermost
985 Carboniferous - Lower Permian of Buxières-les-Mines (Massif Central, France) and
986 the palaeoecology of the European Permo-Carboniferous basins. Neues. Jahrb. Geol.
987 Palaontol. Abh. 232, 325–363.
988 Shackleton, N.J., 1975. Paleotemperature history of the Cenozoic and the initiation of
989 Antarctic glaciation: oxygen and carbon isotope analyses in DSDP sites 277, 279 and
990 281. Init. Repts. DSDP. 29, 743–755.
991 Soler-Gijón, R., 1993. The xenacanth sharks from the Upper Stephanian of the Puertollano
992 basin (Spain). J. Vertebr. Paleontol. 13, 58A.

993 Soler-Gijón, R., 1995. Evidence of predator-prey relationship in xenacanth sharks of the
994 Upper Carboniferous (Stephanian C) from Puertollano, Spain. Geobios. 28, 151–156.
995 Soler-Gijón, R., 1999. Occipital Spine of *Orthacanthus* (Xenacanthidae, Elasmobranchii):
996 Structure and Growth. J. Morphol. 242, 1–45.
997 Soler-Gijón, R., Moratalla, J.J., 2001. Fish and tetrapod trace fossils from the Upper
998 Carboniferous of Puertollano, Spain. Palaeogeogr, Palaeoclimatol, Palaeoecol. 171, 1–
999 28.
1000 Štamberg, S., Schneider, J.W., Werneburg, R., 2016. Fossil fauna and flora of a re-discovered
1001 locality in the Late Carboniferous Ploužnice Horizon of the Krkonoše Piedmont Basin,
1002 Bohemian Massif. Foss. Imp. 72, 215–224.
1003 Steyer, J.-S., Escuillié, F., Pouillon, J.-M., Broutin, J., Debriette, P., Freytet, P., Gand, G.,
1004 Poplin, C., Rage, J.-C., Rival, J., Schneider, J.W., Štamberg, S., Werneburg, R., Cuny,
1005 G., 2000. New data on the flora and fauna from the ?uppermost Carboniferous-Lower
1006 Permian of Buxières-les-Mines, Bourbon l'Archambault Basin (Allier, France).
1007 preliminary report. Bull. Soc. Géol. Fr. 171, 239–249.
1008 Stichler, W., 1995. Interlaboratory comparison of new materials for carbon and oxygen
1009 isotope ratio measurements. Reference and intercomparison materials for stable
1010 isotopes of light elements. 825, 67–74.
1011 Thorrold, S. R., Campana, S. E., Jones, C. M., & Swart, P. K., 1997. Factors determining $\delta^{13}C$
1012 and $\delta^{18}O$ fractionation in aragonitic otoliths of marine fish. Geochim. Cosmochim.
1013 Acta. 61, 2909–2919.
1014 Trotter, J.A., Williams, I.S., Barnes, C.R., Lécuyer, C., Nicoll, R.S., 2008. Did cooling oceans
1015 trigger Ordovician biodiversification? Evidence from conodont
1016 thermometry. Science. 321, 550–554.

Vennemann, T.W., Hegner, E., Cliff, G., Benz, G.W., 2001. Isotopic composition of recent shark teeth as a proxy for environmental conditions. Geochim. Cosmochim. Acta. 65, 1583–1599.

Wenzel, B., Lécuyer, C., Joachimski, M.M., 2008. Comparing oxygen isotope records of Silurian calcite and phosphate—$\delta^{18}O$ compositions of brachiopods and conodonts. Geochim. Cosmochim. Acta. 64, 1859–1872.

Zangerl, R., 1981. Handbook of Paleoichthyology - Chondrichthyes I - Paleozoic Elasmobranchii, Schultze, H.-P., Kuhn, O. (Eds.), Gustav Fischer Verlag, Stuttgart, 115 pp.

Zancolli, G., Steffan-Dewenter, I., Rödel, M.O., 2014. Amphibian diversity on the roof of Africa: unveiling the effects of habitat degradation, altitude and biogeography. Divers. Distrib. 20, 297–308.

Zazzo, A., Lécuyer, C., Sheppard, S.M., Grandjean, P., Mariotti, A., 2004. Diagenesis and the reconstruction of paleoenvironments: a method to restore original $\delta^{18}O$ values of carbonate and phosphate from fossil tooth enamel. Geochim. Cosmochim. Acta. 68, 2245–2258.

Table caption

Table 1. Mean oxygen, carbon and sulfur isotope compositions of the studied vertebrate bioapatites from Buxières-les-Mines and the Muse OSB. The values are those of each specimen. For the single sample specimens (n=1), the standard deviation (sd) equals to the analytical sd of the sample. **Abbreviations: n**, number of samples. **sd**, standard deviation.

Figure captions

1041 **Figure 1.** Geological context. **A**, simplified geological map showing the location of the Autun
1042 and Bourbon l'Archambault basins in the Northern Massif Central. **B**, simplified geological
1043 map of the Autun Basin. **C**, simplified geological map of the Bourbon l'Archambault Basin.
1044 **D**, simplified stratigraphy of the Muse OSB. **E**, simplified stratigraphy of Buxière-les-Mines.
1045 The drawings indicate the known or approximative location of investigated specimens and
1046 taxa. Red stars represent the investigated localities of Buxières-les-Mines and Muse OSB.
1047 **Abbreviations**: **LB**, Lien Blanc; **LV**, Lien Vert (modified from Châteauneuf, 1980; Marteau,
1048 1983; Châteauneuf & Farjanel, 1989; Châteauneuf et al., 1992; Steyer et al., 2000; Gand et
1049 al., 2011, 2015, 2017; Pellenard et al., 2017). [color]
1050
1051 **Figure 2.** Growth pattern of xenacanth dorsal spine and sampling strategy on cf. *Orthacanthus*
1052 sp. (top) and cf. *Triodus* sp. (bottom). The numbers 1 to 12 are the successive analysed samples
1053 from the apex to the base. Dorsal spine drawings are modified from Beck et al. (2016) for cf.
1054 *Orthacanthus* sp. and from Hampe (2003) for cf. *Triodus* sp.
1055
1056 **Figure 3.** Evolution of the $\delta^{18}O_{PO4}$ values along the xenacanth dorsal spines. **A**, cf. *Triodus* sp.
1057 individuals from Muse OSB. **B**, cf. *Orthacanthus* sp. individuals from Buxières-les-Mines. **C**,
1058 cf. *Triodus* sp. specimens from Buxières-les-Mines. [color]
1059
1060 **Figure 4.** Evolution of the $\delta^{13}C_{CO3}$ values along the fin spines of three acanthodian (**A**) and the
1061 dorsal spine of two xenacanth (**B**) individuals from Buxières-les-Mines and the Muse OSB.
1062 [color]
1063
1064 **Figure 5.** Evolution of the $\delta^{34}S$ values along the fin spines of two acanthodian and the dorsal
1065 spine of two xenacanth individuals from Buxières-les-Mines and the Muse OSB. [color]

Figure 6. Evolution of the $\delta^{18}O_{PO4}$ values along seven acanthodian fin spines from Buxières-les-Mines and the Muse OSB. [color]

Figure 7. Oxygen isotope composition of bioapatite phosphate ($\delta^{18}O_{PO4}$) from studied vertebrate taxa plotted against their corresponding oxygen isotope composition of bioapatite carbonate ($\delta^{18}O_{CO3}$). The values are plotted with those (in grey and pink) of modern (Iacumin et., 1996; Vennemann et al., 2001) and fossil (Kolodny and Luz, 1983; Fricke et al., 1998; Lécuyer et al., 2003; Amiot et al., 2010; Goedert et al., 2018) samples from different aquatic environments. The dashed line has a slope of a=1 in order to highlight the correlation between the $d^{18}O_{PO}$ and $d^{18}O_{CO3}$ values. [color]

Figure 8. Difference between the oxygen isotope compositions of bioapatite carbonate ($\delta^{18}O_{CO3}$) and phosphate ($\delta^{18}O_{PO4}$) plotted against the carbonate concentration (CO_3 weight%) of the studied vertebrate taxa. [color]

Figure 9. The sulfur isotope composition of bioapatite ($\delta^{34}S$) plotted against the sulfur content (weight% S) of the studied vertebrate taxa. [color]

Figure 10. Reconstructed palaeotemperature based on the actinopterygians, acanthodians and sharks from Buxières-les-Mines and the Muse OSB. Reconstructed palaeotemperatures using $\delta^{18}O$ of modern marine waters are in the left and those using $\delta^{18}O$ of modern lake waters are in the right. For each taxonomic group, the dot point is the mean value, and the bars represent the standard deviation. Values used can be seen in Table S2. [color]

Figure 11. *Orthacanthus* tooth stuck in a temnospondyl dentary in Buxières-les-Mines. **A**, photograph. **B**, interpretation drawing. [color]

Figure 12. Environmental reconstructions of the Buxières-les-Mines and Muse OSB localities. The presence of the non-investigated cf. *Lissodus* sp. in Buxières-les-Mines follows the faunal list of Steyer et al. (2000). [color]

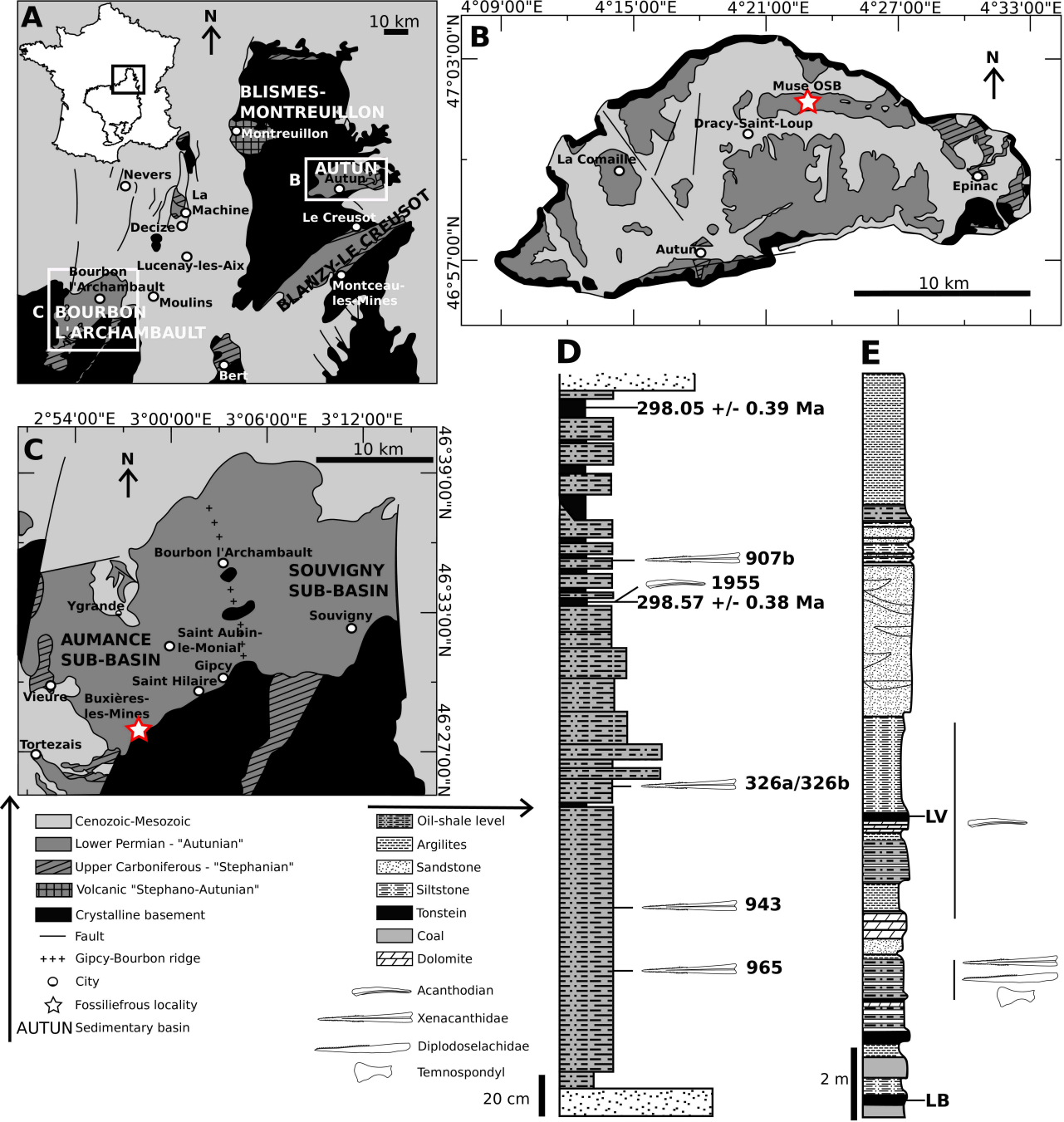
A
N
10 km
BLISMES-
MONTREUILLON
Montreuillon
AUTUN
B
Autun
Nevers
La
Machine
Decize
Le Creusot
Lucenay-les-Aix
Bourbon
l'Archambault
Moulins
C BOURBON
L'ARCHAMBAULT
BLANZY-LE CREUSOT
Montceau-
les-Mines
Bert
4°09'00"E
4°15'00"E
4°21'00"E
4°27'00"E
4°33'00"E
47°03'00"N
46°57'00"N
B
N
Muse OSB
Dracy-Saint-Loup
La Comaille
Epinac
Autun
10 km
2°54'00"E
3°00'00"E
3°06'00"E
3°12'00"E
46°39'00"N
46°33'00"N
46°27'00"N
C
N
10 km
Bourbon l'Archambault
SOUVIGNY
SUB-BASIN
Souvigny
Ygrande
AUMANCE
SUB-BASIN
Saint Aubin-
le-Monial
Gipcy
Saint Hilaire
Vieure
Buxières-
les-Mines
Tortezais
Cenozoic-Mesozoic
Lower Permian - "Autunian"
Upper Carboniferous - "Stephanian"
Volcanic "Stephano-Autunian"
Crystalline basement
Fault
Gipcy-Bourbon ridge
City
Fossiliefrous locality
AUTUN Sedimentary basin
Oil-shale level
Argilites
Sandstone
Siltstone
Tonstein
Coal
Dolomite
Acanthodian
Xenacanthidae
Diplodoselachidae
Temnospondyl
20 cm
D
298.05 +/- 0.39 Ma
907b
1955
298.57 +/- 0.38 Ma
326a/326b
943
965
E
LV
2 m
LB

A

Muse OSB

cf. *Triodus* sp.

326a/326b

907b

965a

943

$\delta^{18}O_{PO4}$ (‰ V-SMOW)

Distance to apex (cm)

B

Buxières-les-Mines

cf. *Orthacanthus* sp.

D13

BX04

$\delta^{18}O_{PO4}$ (‰ V-SMOW)

Distance to apex (cm)

C

D11

D08

D07

BX28

BX23b

BX23a

Buxières-les-Mines

cf. *Triodus* sp.

$\delta^{18}O_{PO4}$ (‰ V-SMOW)

Distance to apex (cm)

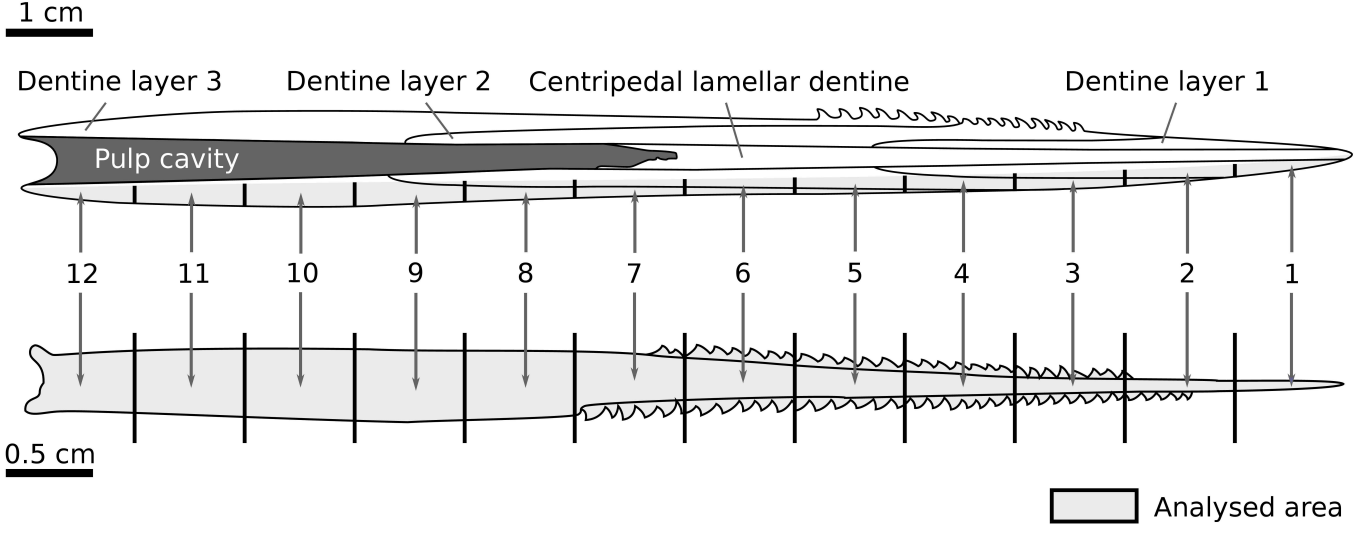
1 cm
Dentine layer 3
Dentine layer 2
Centripedal lamellar dentine
Dentine layer 1
Pulp cavity
12
11
10
9
8
7
6
5
4
3
2
1
0.5 cm
Analysed area

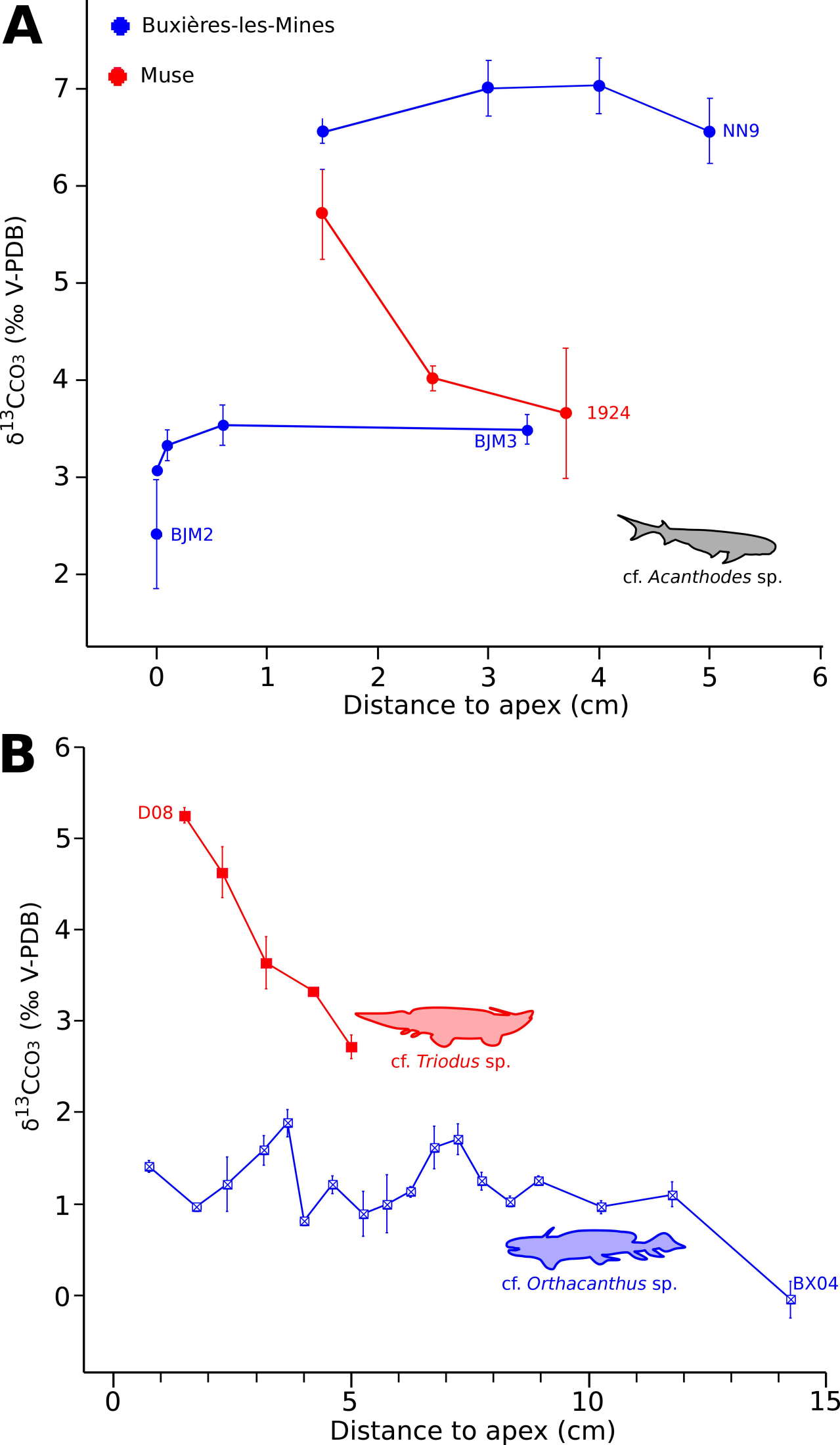
A
Buxières-les-Mines
Muse
NN9
1924
BJM3
BJM2
cf. Acanthodes sp.
δ13CCO3 (‰ V-PDB)
Distance to apex (cm)
B
D08
cf. Triodus sp.
cf. Orthacanthus sp.
BX04
δ13CCO3 (‰ V-PDB)
Distance to apex (cm)

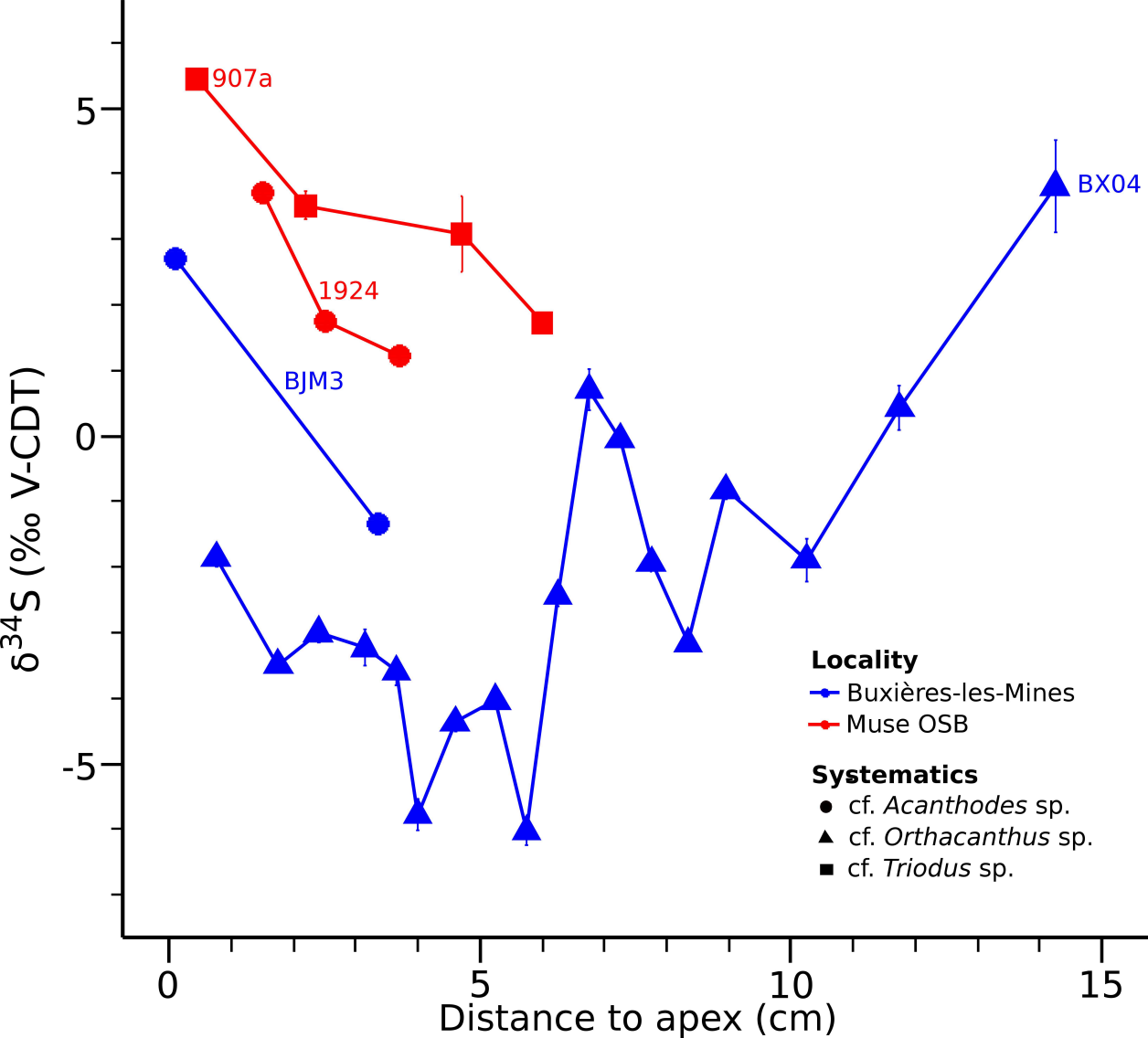
907a
1924
BJM3
BX04
5
0
-5
0
5
10
15
δ34S (‰ V-CDT)
Distance to apex (cm)
Locality
Buxières-les-Mines
Muse OSB
Systematics
cf. Acanthodes sp.
cf. Orthacanthus sp.
cf. Triodus sp.

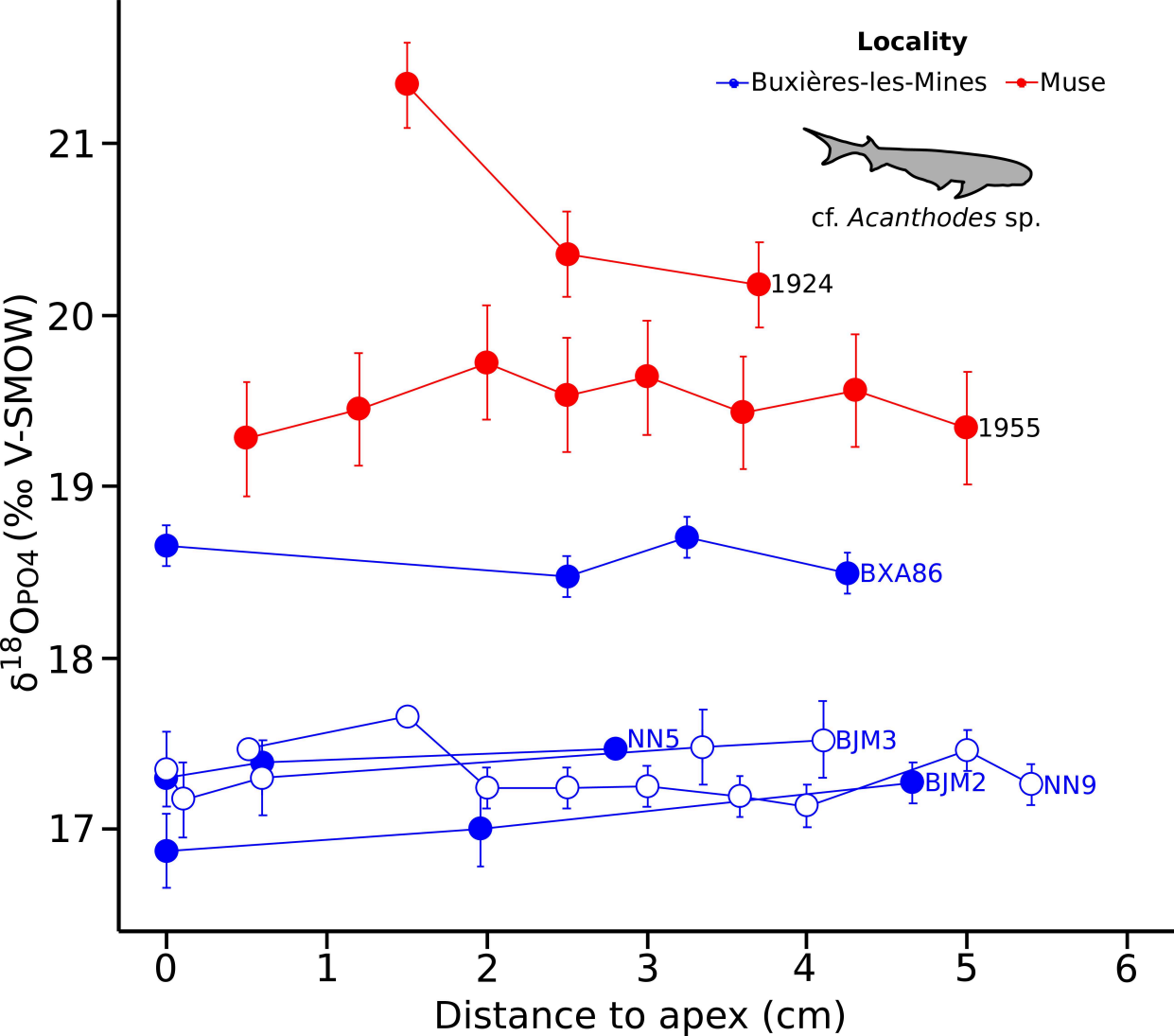
Locality
Buxières-les-Mines
Muse
cf. Acanthodes sp.
1924
1955
BXA86
NN5
BJM3
BJM2
NN9
δ18OPO4 (‰ V-SMOW)
Distance to apex (cm)
21
20
19
18
17
0
1
2
3
4
5
6

Modern freshwater stingrays tolerance

Modern tropical actinopterygian tolerance

Buxières-les-Mines

Greenhouse | Icehouse | Matano | Punta Laguna | Tanganyika

Temperature (°C)

40 38 36 34 32

44 42 40 38 36

24 22 20 18 16

48 46 44 42 40

62 60 58 56 54

Temperature (°C)

Muse OSB

Greenhouse | Icehouse | Matano | Punta Laguna | Tanganyika

Temperature (°C)

35 30 25 20 15 10

40 35 30 25 20 15

20 15 10 5 0 -5

45 40 35 30 25 20

60 55 50 45 40 35

Temperature (°C)

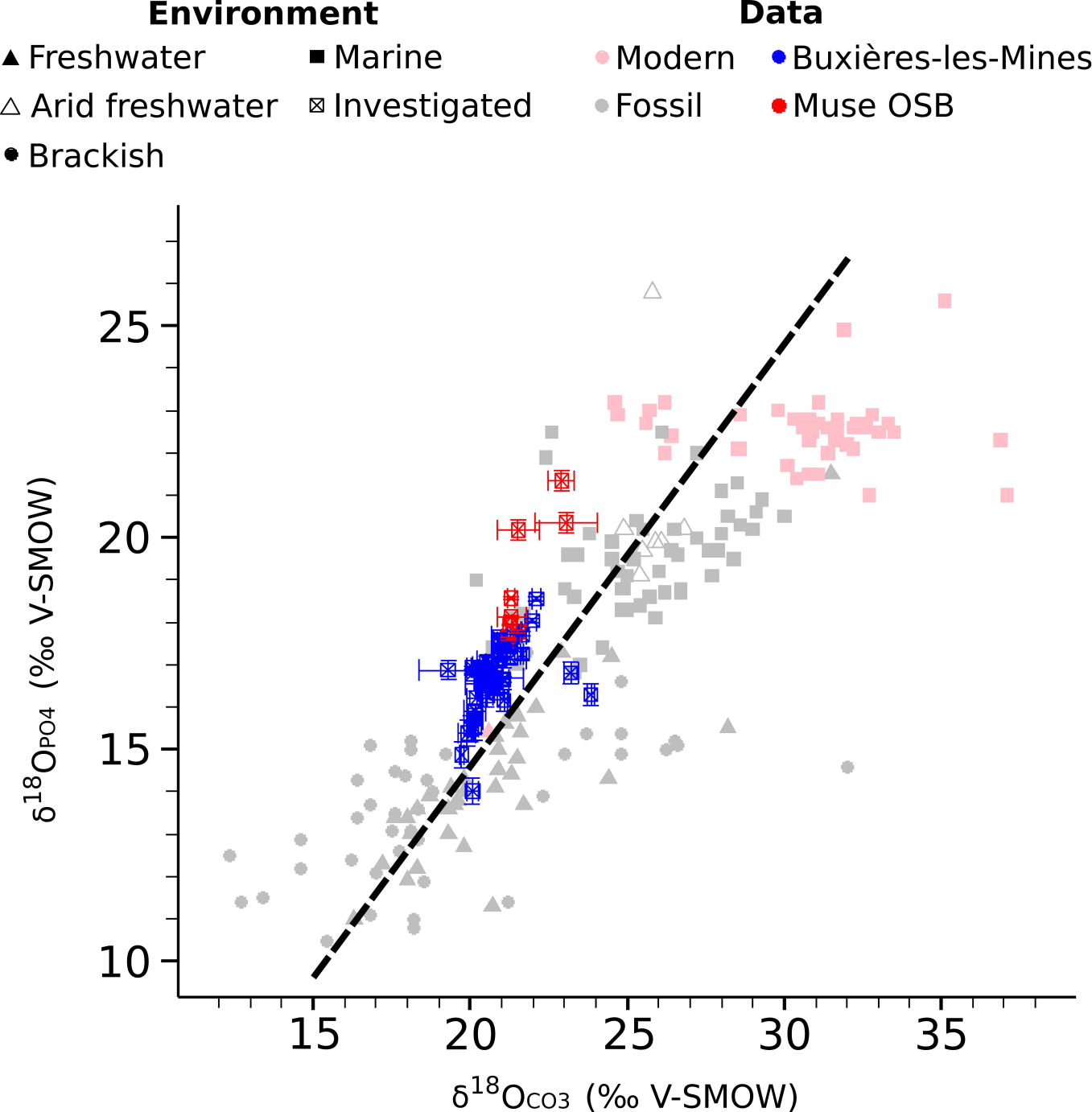
Environment
Freshwater
Arid freshwater
Brackish
Marine
Investigated
Data
Modern
Fossil
Buxières-les-Mines
Muse OSB
δ18OPO4 (‰ V-SMOW)
δ18OCO3 (‰ V-SMOW)
10
15
20
25
15
20
25
30
35

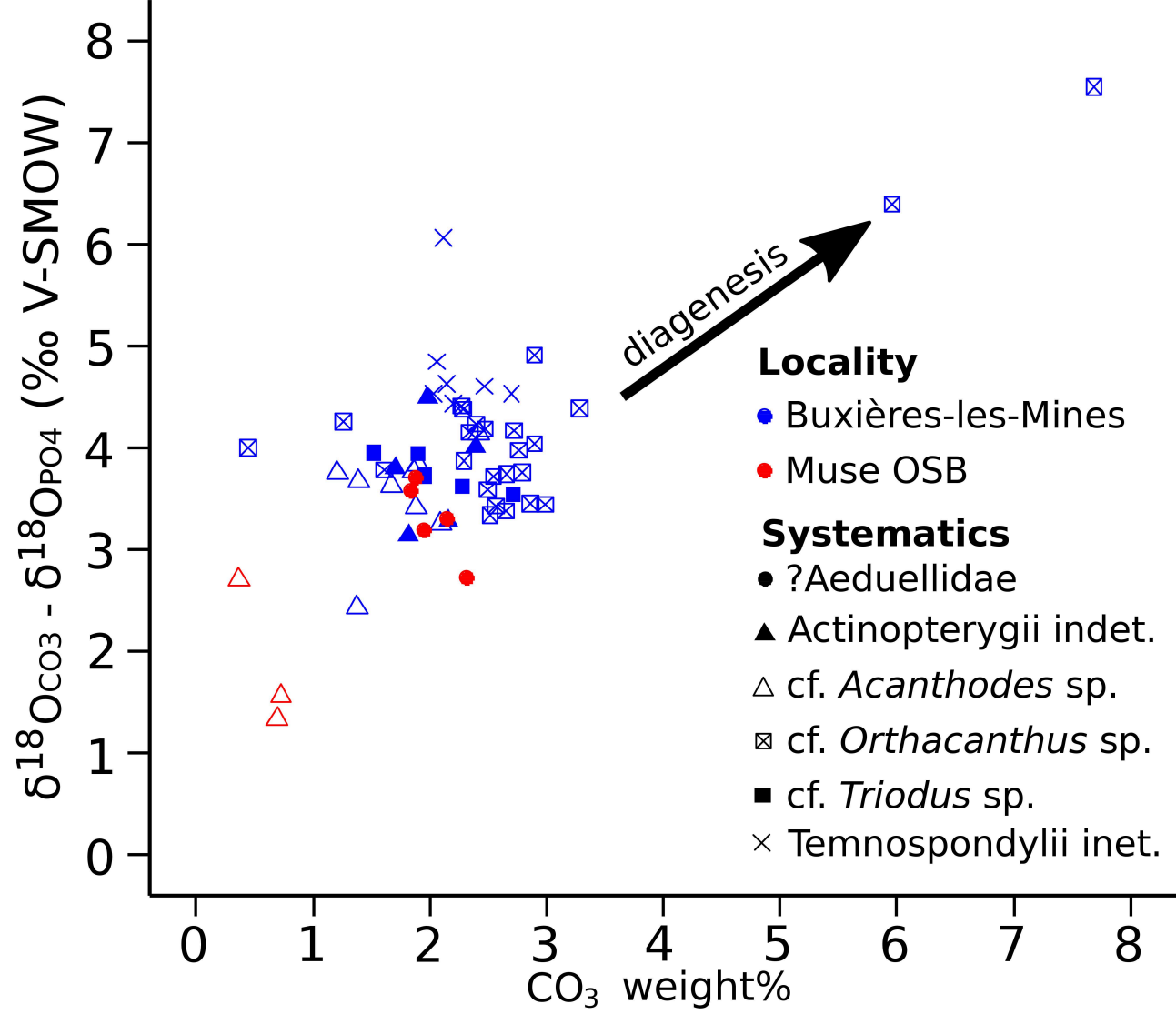
$\delta^{18}O_{CO3}$ - $\delta^{18}O_{PO4}$ (‰ V-SMOW)
CO_3 weight%
diagenesis
Locality
Buxières-les-Mines
Muse OSB
Systematics
?Aeduellidae
Actinopterygii indet.
cf. *Acanthodes* sp.
cf. *Orthacanthus* sp.
cf. *Triodus* sp.
Temnospondylii inet.

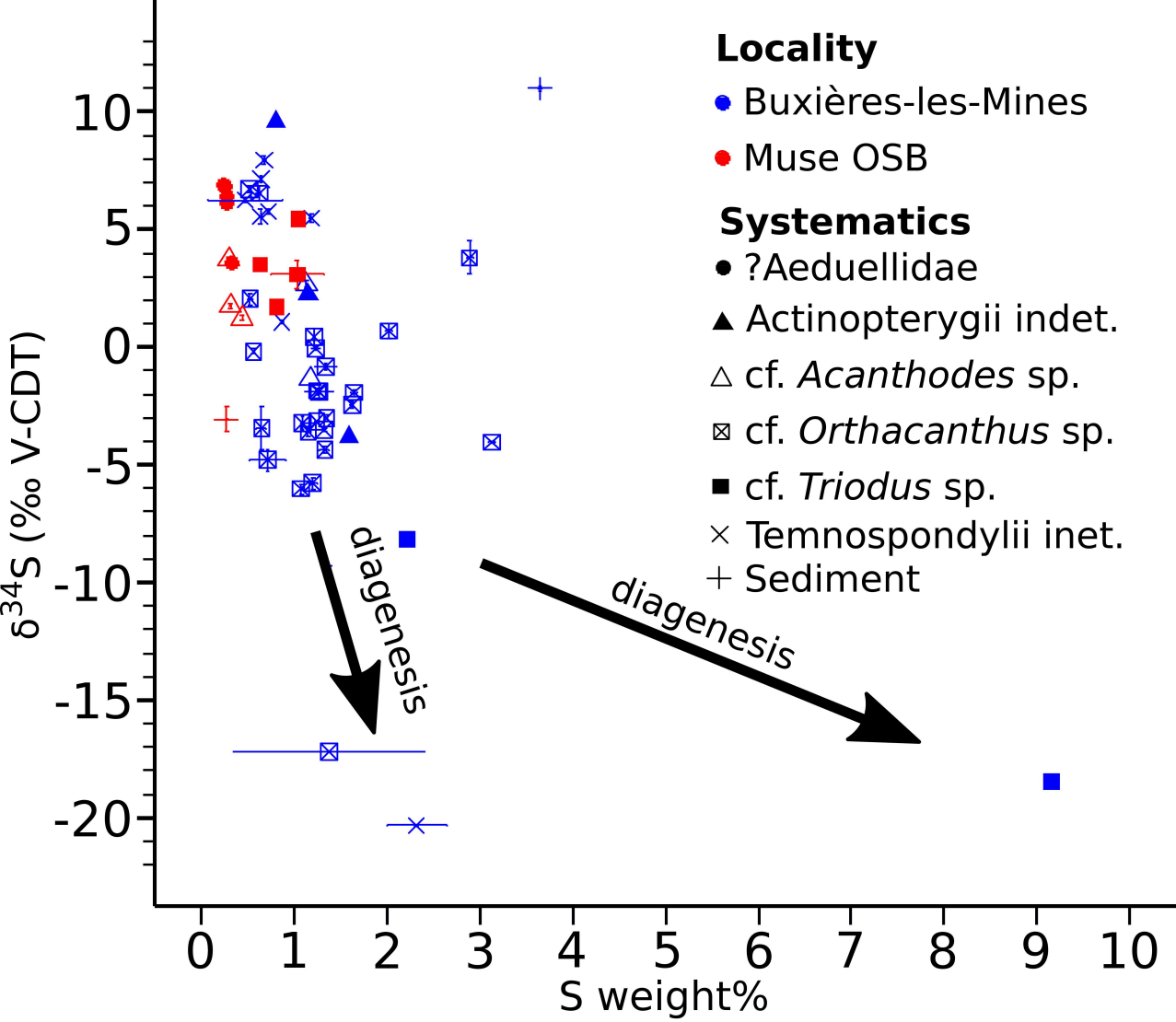
Locality
Buxières-les-Mines
Muse OSB
Systematics
?Aeduellidae
Actinopterygii indet.
cf. Acanthodes sp.
cf. Orthacanthus sp.
cf. Triodus sp.
Temnospondylii inet.
Sediment
diagenesis
diagenesis
δ34S (‰ V-CDT)
S weight%
10
5
0
-5
-10
-15
-20
0
1
2
3
4
5
6
7
8
9
10


A
1 cm

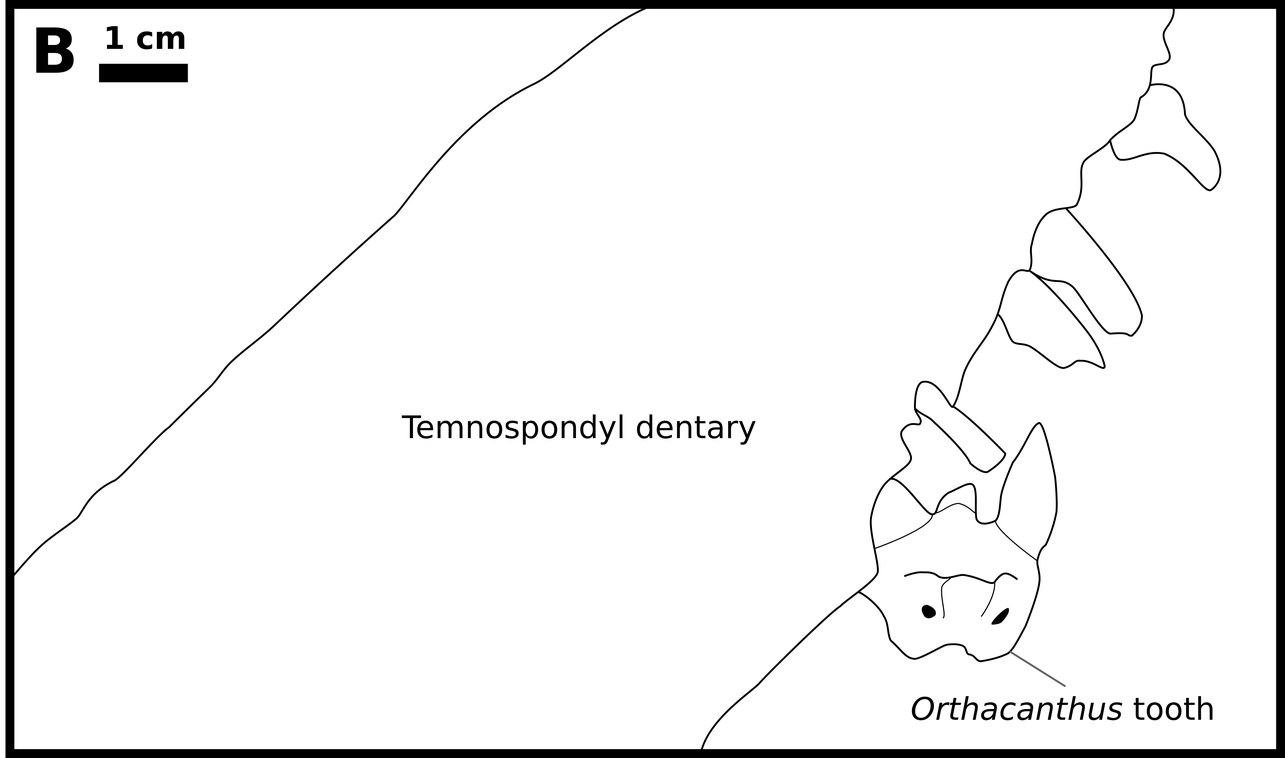
B
1 cm
Temnospondyl dentary
Orthacanthus tooth

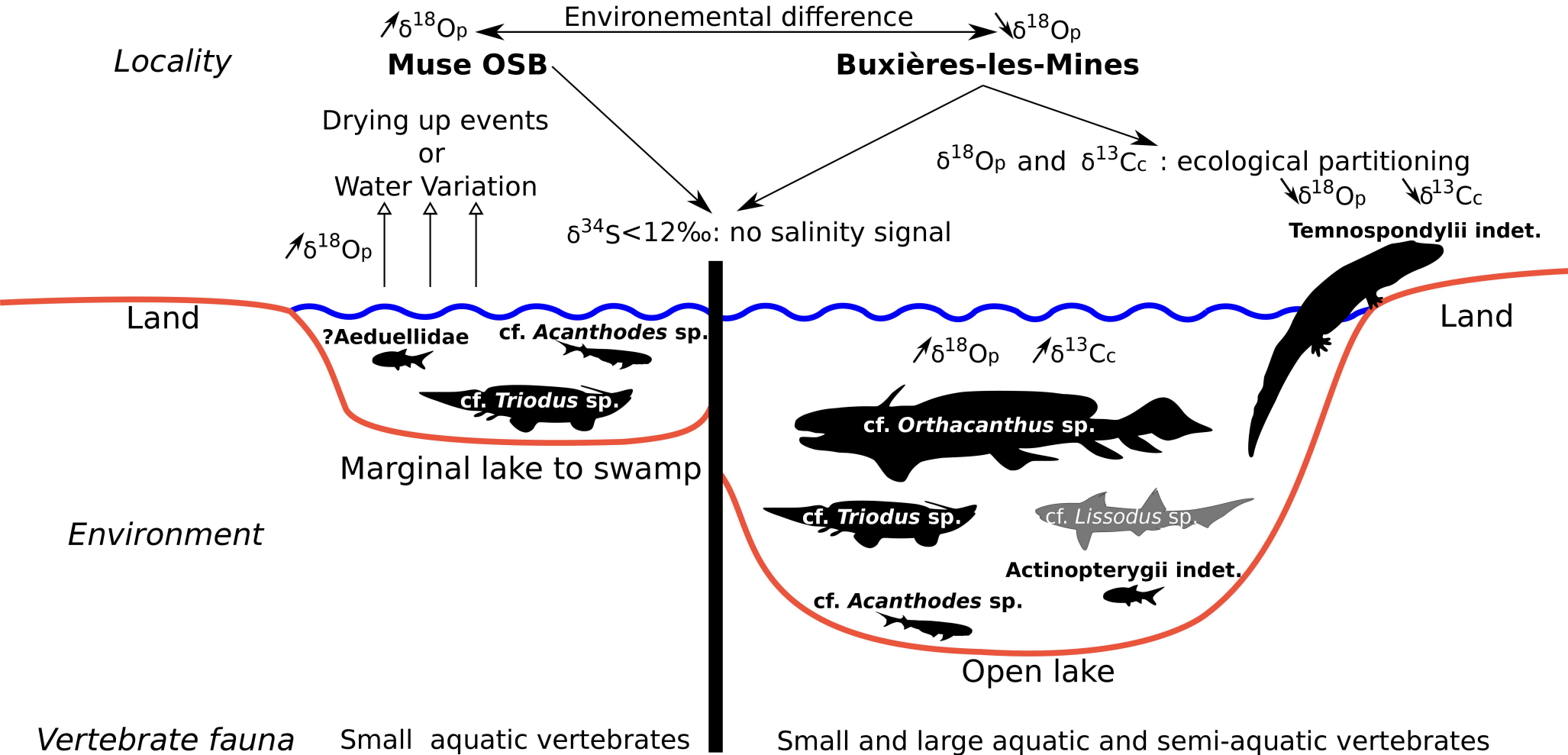
Locality
↗δ18Op
Environemental difference
↘δ18Op
Muse OSB
Buxières-les-Mines
Drying up events
or
Water Variation
↗δ18Op
δ34S<12‰: no salinity signal
δ18Op and δ13Cc : ecological partitioning
↘δ18Op
↘δ13Cc
Temnospondylii indet.
Land
Land
?Aeduellidae
cf. Acanthodes sp.
cf. Triodus sp.
Marginal lake to swamp
↗δ18Op
↗δ13Cc
cf. Orthacanthus sp.
cf. Triodus sp.
cf. Lissodus sp.
Actinopterygii indet.
cf. Acanthodes sp.
Open lake
Environment
Vertebrate fauna
Small aquatic vertebrates
Small and large aquatic and semi-aquatic vertebrates